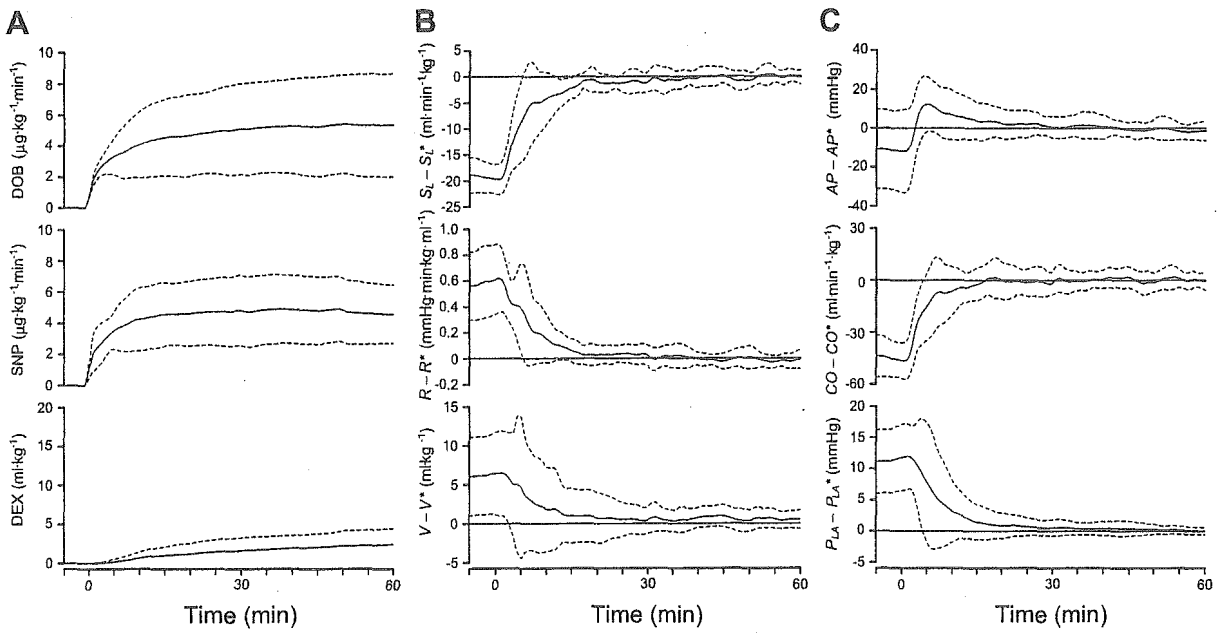

Fig. 5. Time courses of infusion rates of Dob and SNP, and cumulated volume of infused Dex (*A*), differences between measured and target cardiovascular parameters (*B*), and differences between measured and target hemodynamic variables (*C*) averaged for 12 dogs during closed-loop control of hemodynamics. Data are expressed as mean (solid line) ± SD (broken line). As the differences between measured and target parameters converged to the zero lines, the differences between measured and target hemodynamic variables also converged to the zero lines and remained at those levels.

respectively. The average standard deviations from the target values were small for AP [4.4 mmHg (SD 2.6)], CO [5.4 $ml \cdot min^{-1} \cdot kg^{-1}$ (SD 2.4)] and Pla [0.8 mmHg (SD 0.6)]. In case of severe hypotension, restoring normal AP should be done within a few minutes to prevent cerebral ischemia. Four of 12 dogs exhibited severe hypotension [AP, 67 mmHg (SD 6)]. In these animals, AP* [95 mmHg (SD 4)] was attained within 4 min [mean 2.8 min (SD 0.7)]. Hemodynamic data before, during, and after the closed-loop control of hemodynamics are summarized in Table 3. After the system was turned off, AP, CO, and Pla gradually returned to their precontrol levels in 11 animals. In one animal, however, progressive hypotension followed by intractable ventricular fibrillation occurred ~3 min after the system was turned off.

In two dogs (*group 2*), AP, CO, and Pla were controlled with reasonable stability over a longer periods of time (100–150 min). Standard deviations from target values were small for AP (3.9–7.8 mmHg), CO (2.7–6.6 $ml \cdot min^{-1} \cdot kg^{-1}$), and Pla (0.7–2.5 mmHg).

Table 3. *Hemodynamic data before, during, and after the closed-loop control of hemodynamics*

	Before (n = 12)	During (n = 12)	After (n = 11)
HR, beats/mm	147.4 (26.8)	149.4 (25.0)	135.7 (25.2)†‡
AP, mmHg	86.7 (22.4)	97.0 (7.4)	75.2 (21.1)‡
CO, $ml \cdot min^{-1} \cdot kg^{-1}$	53.7 (14.6)	96.7 (5.3)†	53.5 (8.6)‡
Pla, mmHg	21.8 (5.5)	10.8 (1.2)†	18.5 (3.4)‡
Pra, mmHg	6.9 (1.8)	4.4 (0.9)†	7.4 (2.2)‡
S_L, $ml \cdot min^{-1} \cdot kg^{-1}$	14.3 (4.0)	32.7 (2.6)†	15.1 (2.9)‡
R, $mmHg \cdot min \cdot ml^{-1} \cdot kg$	1.5 (0.3)	1.0 (0.1)†	1.3 (0.4)*‡
V, ml/kg	34.2 (4.9)	28.5 (2.3)†	34.0 (5.4)‡

Values are means (SD). *$P < 0.05$, †$P < 0.01$ vs. Before; ‡$P < 0.01$ vs. During.

DISCUSSION

To the best of our knowledge, the automated drug delivery system we have developed is the first to successfully control AP, CO, and Pla simultaneously with reasonably good accuracy and stability. In a canine model of acute heart failure, our system automatically normalizes AP, CO, and Pla and maintains the levels stably within the desired ranges. Therefore, our system is potentially useful in the management of patients with acute decompensated heart failure.

Previous Closed-Loop Systems Controlling Hemodynamic Variables

Several previous systems have attempted to control two hemodynamic variables simultaneously (18, 26, 27). However, it is difficult to expand them to closed-loop control of the overall hemodynamics.

Voss et al. (26) and Yu et al. (27) reported closed-loop systems to control AP and CO using inotropes and vasodilators in dogs. In these systems, all possible input-output relations between drug infusion and the response of the controlled variable have to be estimated; namely, inotrope-AP, inotrope-CO, vasodilator-AP, and vasodilator-CO relations. The reason for this is that these drugs affect AP and CO simultaneously to almost the same degree. If this approach is applied to simultaneous control of AP, CO, and Pla, at least nine input-output relations have to be estimated, because at least three drugs are required to independently control the three variables. This would make the system extremely complicated and therefore be practically unfeasible.

In addition, the input-output relations must be estimated online in individual animals to tune the drug controllers. The reason for this is that the relations differ widely between animals and within animal over time. Even the direction of the

output response can change. For example, CO usually increases in response to SNP infusion in subjects with failing hearts but may also decrease in subjects with preserved cardiac function (23, 26). In the closed-loop system of Voss et al., such estimation induced unacceptably large fluctuations in AP (26). The feasibility of such online estimation is questionable when drug infusion rates are allowed to vary simultaneously because of the difficulty to differentiate between drug effects. To avoid this problem, Hoeksel et al. (18) allowed only one drug to be varied at a time, whereas other drugs were kept constant in closed-loop control of AP and pulmonary arterial pressure during cardiac surgery. However, their adjustments of volume supplementation or dobutamine infusion were manual. Their system did not completely automate the control of hemodynamics.

Characteristics of Our System

Our system controls the cardiovascular parameters characterizing the integrated CO curve, venous return surface, and arterial resistance and as a result achieves target values for hemodynamic variables. Compared with previous systems, our system may appear to adopt a rather roundabout approach. Our concept is that controlling the cardiovascular parameters is physiologically more rational, because it is equivalent to directly controlling the mechanical determinants of circulation. As indicated by Guyton et al. (16, 17), when the mechanics of the circulation are considered, the hemodynamic variables such as AP, CO, and atrial pressures are the effects, or dependent variables. Blood volume and the mechanical properties of the heart and vasculature, such as heart rate, ventricular contractility, and vascular resistance, are the causes, or independent variables. The integrated CO curve and venous return surface display these properties through the relationship between the flow and atrial pressures (24, 25). The total artificial heart control system developed by Abe et al. (1) adjusted its output in accordance with the vascular conductance (1/resistance) and AP, thereby achieving appropriate response to peripheral metabolic demands and avoiding hemodynamic abnormalities exhibited by other total artificial heart control systems. Their results also suggest that it is essential to consider the mechanical determinant of circulation for the control of the hemodynamic variables.

Our approach is advantageous from the perspective of control engineering. The three drug controllers (Fig. 2*A*) are designed on the basis of only four input-output relations between the drug infusion and the response of the controlled parameter; namely, Dob-S_L, SNP-R, Dex-V, and Fur-V (Fig. 3). We also found that Dob decreases R and increases V, and SNP increases S_L and decreases V (data not shown), which are compatible with previous studies (7, 22, 23). If these secondary effects induce significant interactions among the three closed loops, additional controllers would be needed to compensate for the interactions (4). However, our results indicate that these secondary effects are small enough to be compensated by the three drug controllers, and additional controllers are not necessary. The fact that the three closed loops are effectively decoupled drastically simplifies the entire system. This also permits system operators to understand its behavior easily (4).

Although we fix the PI gain constants and the constants of if-then rules, controls of cardiovascular parameters are accurate and stable (Fig. 4*B*). There are interindividual differences in the response of the parameters to drug infusion (Fig. 3). There should also be intraindividual differences in the response over time. However, our results indicate that the three drug controllers effectively compensate for all of these differences and do not require adaptive tuning in individual animals as in the previous system. As long as each cardiovascular parameter responds sensitively to the corresponding agent, our system is able to achieve target values for all the parameters, thereby achieving target hemodynamic variables.

Our system explicitly quantifies cardiac pump function, preload, and afterload, thereby controlling the overall hemodynamics. We believe that this unique feature of our system is intuitively appealing and is acceptable to clinicians.

Clinical Application of Our System

Our system will reduce the stress and work imposed on physicians and nurses who are managing patients with unstable hemodynamic conditions. These personnel will be able to spend more time on other patient-related activities, thereby improving the quality of patient care (10, 11). We believe that the closed-loop control of overall hemodynamics can extend the improvement in postoperative outcome demonstrated by Chitwood et al. (10) to various aspects of clinical cardiology or cardiac surgery.

In clinical settings, multisystem disorders such as renal disease, anemia, and diabetes may affect the performance of our system. Renal disease can weaken the response of V to the infusion of Fur. The hemodynamic changes in anemia include increased preload and reduced arterial resistance as compensatory mechanisms for the reduced oxygen-carrying capacity of the blood (8). These changes may affect the control of V and R by our system. In patients with diabetic cardiomyopathy, the sensitivity of S_L to Dob infusion may be reduced (5). Drugs prescribed before hospitalization such as β-blockers, or used during hospitalization such as morphine may also affect the performance of our system. Chronic β-adrenergic blockade can weaken the sensitivity of S_L to Dob infusion (2). Administration of morphine may change the response of V and R to the drugs infused (15). We must clarify these effects on the performance of our system as thoroughly as possible before our system can be considered for clinical application.

In the routine clinical environment, CO, and pulmonary artery occlusion pressure, a substitute for Pla, are measured intermittently with a Swan-Ganz catheter. For clinical application of our system, it is a prerequisite to monitor these variables continuously. Several methods have been developed to continuously monitor CO or the pulmonary artery occlusion pressure (6, 12). Integrating these methods into our system would bring the clinical application of our system closer to reality.

Limitations

All the experiments of this study were conducted in anesthetized, open-chest dogs. Anesthesia and surgical trauma affect the cardiovascular system significantly. Whether the present system is efficacious in conscious, closed-chest animals (including humans) remains to be seen.

We parameterized the integrated cardiac output curve and the venous return surface using *Eqs. A1*, *A2*, and *A4* (24, 25). Even if the actual curve or surface deviate slightly from those

estimated by these equations, our system compensates such deviations by the negative feedback mechanism. However, we did not confirm whether the estimation works well outside the physiological ranges of Pla and Pra, particularly under low atrial pressures (24, 25). The efficacy of our system in such conditions remains to be evaluated.

Our system controls R with vasodilators only and lacks a controller to increase R with vasoconstrictors. This will not be a major problem because the pathophysiology of acute heart failure is characterized by excessive vasoconstriction due to enhanced activity of sympathetic and renin-angiotensin systems (19). Vasoconstrictor control is necessary, however, for the management of patients with excessive vasodilatation, such as those in septic shock (21).

In this study, control of S_L was accurate and stable. However, it would be impossible to restore S_L pharmacologically if S_L is more severely depressed than those seen in this study as in the case of more diffuse myocardial disease or superimposed coronary artery disease. We must clarify in future studies to what magnitude of S_L depression can our system restore it reliably. In addition, how to use our system with mechanical circulatory support such as the intra-aortic balloon pump in case of the severe S_L depression remains to be established.

In the present design, if S_L is unable to respond to the infusion of Dob, the system will automatically increase the infusion rate of Dob owing to its negative feedback mechanism. This would be problematic especially in case of arrhythmia, which is a serious noise in the closed-loop control of S_L. If not appropriately suppressed, frequent premature ventricular contractions or ventricular tachycardia will depress S_L owing to disorganized ventricular contraction. In response to the depressed S_L, the system automatically increases the infusion rate of dobutamine. This could further exacerbate the arrhythmia, thus leading to a vicious cycle and collapse of the hemodynamics. To prevent such malfunction, a smart "sensor" that will filter these unwanted artifacts should be included in our system.

In the present study, we recorded only the urine volume. Measurement of urine flow and sodium excretion is essential to evaluate renal function, which is a very important prognostic indicator in patients with acute decompensated heart failure (14). It would be desirable to add the monitoring of these parameters to our system to improve the quality of patient care.

In conclusion, by directly controlling the mechanical determinants of circulation, our automated drug delivery system allows simultaneous control of AP, CO, and Pla with reasonable accuracy and stability and is potentially a powerful clinical tool for the management of patients with acute decompensated heart failure.

APPENDIX A

Parameters of Integrated Cardiac Output Curve, Venous Return Surface, and Arterial Resistance

We parameterized the integrated CO curve, the venous return surface and the systemic arterial resistance on the basis of previous studies (24, 25). In the integrated CO curve, CO ($ml \cdot min^{-1} \cdot kg^{-1}$) is closely related to Pla (mmHg) by the following formula (24):

$$CO = S_L \times [\ln(Pla - 2.03) + 0.80] \quad (A1)$$

and CO to Pra (mmHg) as follows:

$$CO = S_R \times [\ln(Pra - 1.0) + 0.88] \quad (A2)$$

S_L and S_R ($ml \cdot min^{-1} \cdot kg^{-1}$) are parameters representing the preload sensitivity of CO, i.e., the pumping ability of the left and right heart, respectively. These relations are consistent among different animals (24). In a preliminary study, we found that the ratio of S_R to S_L (α) remains fairly constant during infusion of dobutamine (data not shown). This suggests that once we know α, we can predict S_R in relation to a known change in S_L. Therefore we used S_L to parameterize the integrated CO curve. S_L can be calculated from CO and Pla by rewriting *Eq. A1* as follows:

$$S_L = CO/[\ln(Pla - 2.03) + 0.80] \quad (A3)$$

The venous return surface can be mathematically expressed by the following formula (25):

$$CO_V = V/0.129 - 19.61Pra - 3.49Pla \quad (A4)$$

V (ml/kg) is total stressed blood volume, and CO_V ($ml \cdot min^{-1} \cdot kg^{-1}$) is integrated venous return from systemic and pulmonary circulations. This relationship is also consistent among different animals (25). We used V to parameterize the venous return surface. V can be calculated from CO (= CO_V), Pla, and Pra by rewriting *Eq. A4* as follows:

$$V = (CO + 19.61Pra + 3.49Pla) \times 0.129 \quad (A5)$$

We parameterized the systemic arterial resistance (R) ($mmHg \cdot ml^{-1} \cdot min \cdot kg$) by the following formula:

$$R = (AP - Pra)/CO \quad (A6)$$

APPENDIX B

Determination of Target Parameters

On the basis of AP*, CO*, and Pla*, our system determines S_L*, V*, and R* as follows: S_L* is calculated by substituting CO* and Pla* into *Eq. A3*. By substituting baseline CO, Pla, and Pra into *Eqs. A1* and *A2*, baseline S_L and S_R are calculated to determine α. S_R (S_R*) corresponding to S_L* is predicted as:

$$S_R^* = \alpha \cdot S_L^* \quad (B1)$$

From *Eq. A2* and *B1*, target Pra (Pra*) is predicted as:

$$Pra^* = \exp[(CO^*)/(S_R^*) - 0.88] + 1.0 \quad (B2)$$

By substituting CO*, Pla*, and Pra* into *Eq. A5*, V* can be determined. By substituting AP*, CO*, and Pra* into *Eq. A6*, R* can be calculated.

GRANTS

This study was supported by Grant-in-Aid for Young Scientists (B) (16700379) from the Ministry of Education, Culture, Sports, Science and Technology, by Health and Labour Sciences Research Grants for Research on Medical Devices for Analyzing, Supporting and Substituting the Function of Human Body (H15-physi-001) from the Ministry of Health Labour and Welfare of Japan, and by the Program for Promotion of Fundamental Studies in Health Science of the National Institute of Biomedical Innovation. This study was also conducted as a part of "Ground-based Research Announcement for Space Utilization" promoted by Japan Space Forum.

REFERENCES

1. **Abe Y, Chinzei T, Mabuchi K, Snyder AJ, Isoyama T, Imanishi K, Yonezawa T, Matsuura H, Kouno A, Ono T, Atsumi K, Fujimasa I, and Imachi K.** Physiological control of a total artificial heart: conductance- and arterial pressure-based control. *J Appl Physiol* 84: 868–876, 1998.
2. **Antman EM, Anbe DT, Armstrong PW, Bates ER, Green LA, Hand M, Hochman JS, Krumholz HM, Kushner FG, Lamas GA, Mullany CJ, Ornato JP, Pearle DL, Sloan MA, and Smith SC Jr; American College of Cardiology; American Heart Association; Canadian Car-**

diovascular Society. ACC/AHA guidelines for the management of patients with ST-elevation myocardial infarction—executive summary. A report of the American College of Cardiology/American Heart Association Task Force on Practice Guidelines (Writing Committee to revise the 1999 guidelines for the management of patients with acute myocardial infarction). *J Am Coll Cardiol* 44: 671–719, 2004.

3. **Arakawa M, Jerome EH, Enzan K, Grady M, and Staub NC.** Effects of dextran 70 on hemodynamics and lung liquid and protein exchange in awake sheep. *Circ Res* 67: 852–861, 1990.
4. **Astrom KJ and Hagglund T.** *PID Controller: Theory, Design, and Tuning* (2nd ed.). Research Triangle Park, NC: Instrument Society of America, 1995, p. 59–199.
5. **Atkins FL, Dowell RT, and Love S.** β-Adrenergic receptors, adenylate cyclase activity, and cardiac dysfunction in the diabetic rat. *J Cardiovasc Pharmacol* 7: 66–70, 1985.
6. **Bein B, Worthmann F, Tonner PH, Paris A, Steinfath M, Hedderich J, and Scholz J.** Comparison of esophageal Doppler, pulse contour analysis, and real-time pulmonary artery thermodilution for the continuous measurement of cardiac output. *J Cardiothorac Vasc Anesth* 18: 185–189, 2004.
7. **Binkley PF, Murray KD, Watson KM, Myerowitz PD, and Leier CV.** Dobutamine increases cardiac output of the total artificial heart. Implications for vascular contribution of inotropic agents to augmented ventricular function. *Circulation* 84: 1210–1215, 1991.
8. **Chapler CK and Cain SM.** The physiologic reserve in oxygen carrying capacity: studies in experimental hemodilution. *Can J Physiol Pharmacol* 64: 7–12, 1986.
9. **Chien KL, Hrones JA, and Reswick JB.** On the automatic control of generalized passive systems. *Trans ASME* 74: 175–185, 1952.
10. **Chitwood WR Jr, Cosgrove DM III, and Lust RM.** Multicenter trial of automated nitroprusside infusion for postoperative hypertension. Titrator Multicenter Study Group. *Ann Thorac Surg* 54: 517–522, 1992.
11. **Cosgrove DM III, Petre JH, Waller JL, Roth JV, Shepherd C, and Cohn LH.** Automated control of postoperative hypertension: a prospective, randomized multicenter study. *Ann Thorac Surg* 47: 678–682, 1989.
12. **DeBoisblanc BP, Pellett A, Johnson R, Champagne M, McClarty E, Dhillon G, and Levitzky M.** Estimation of pulmonary artery occlusion pressure by an artificial neural network. *Crit Care Med* 31: 261–266, 2003.
13. **Forrester JS, Diamond G, Chatterjee K, and Swan HJ.** Medical therapy of acute myocardial infarction by application of hemodynamic subsets (first of two parts). *N Engl J Med* 295: 1356–1362, 1976.
14. **Gottlieb SS, Abraham W, Butler J, Forman DE, Loh E, Massie BM, O'Connor CM, Rich MW, Stevenson LW, Young J, and Krumholz HM.** The prognostic importance of different definitions of worsening renal function in congestive heart failure. *J Card Fail* 8: 136–141, 2002.
15. **Greenberg S, McGowan C, Xie J, and Summer WR.** Selective pulmonary and venous smooth muscle relaxation by furosemide: a comparison with morphine. *J Pharmacol Exp Ther* 270: 1077–1085, 1994.
16. **Guyton AC.** Determination of cardiac output by equating venous return curves with cardiac response curves. *Physiol Rev* 35: 123–129, 1955.
17. **Guyton AC, Coleman TG, and Granger HJ.** Circulation: overall regulation. *Annu Rev Physiol* 34: 13–46, 1972.
18. **Hoeksel SA, Blom JA, Jansen JR, Maessen JG, and Schreuder JJ.** Automated infusion of vasoactive and inotropic drugs to control arterial and pulmonary pressures during cardiac surgery. *Crit Care Med* 27: 2792–2798, 1999.
19. **Johnson W, Omland T, Hall C, Lucas C, Myking OL, Collins C, Pfeffer M, Rouleau JL, and Stevenson LW.** Neurohormonal activation rapidly decreases after intravenous therapy with diuretics and vasodilators for class IV heart failure. *J Am Coll Cardiol* 39: 1623–1629, 2002.
20. **Kaplan JA and Guffin AV.** Treatment of perioperative left ventricular failure. In: *Cardiac Anesthesia* (3rd ed.), edited by Kaplan JA. Philadelphia, PA: Saunders, 1993, p. 1058–1094.
21. **Martin C, Viviand X, Arnaud S, Vialet R, and Rougnon T.** Effects of norepinephrine plus dobutamine or norepinephrine alone on left ventricular performance of septic shock patients. *Crit Care Med* 27: 1708–1713, 1999.
22. **Ogilvie RI and Zborowska-Sluis D.** Effects of nitroglycerin and nitroprusside on vascular capacitance of anesthetized ganglion-blocked dogs. *J Cardiovasc Pharmacol* 18: 574–580, 1991.
23. **Pouleur H, Covell JW, and Ross J Jr.** Effects of nitroprusside on venous return and central blood volume in the absence and presence of acute heart failure. *Circulation* 61: 328–337, 1980.
24. **Uemura K, Kawada T, Kamiya A, Aiba T, Hidaka I, Sunagawa K, and Sugimachi M.** Prediction of circulatory equilibrium in response to changes in stressed blood volume. *Am J Physiol Heart Circ Physiol* 289: H301–H307, 2005.
25. **Uemura K, Sugimachi M, Kawada T, Kamiya A, Jin Y, Kashihara K, and Sunagawa K.** A novel framework of circulatory equilibrium. *Am J Physiol Heart Circ Physiol* 286: H2376–H2385, 2004.
26. **Voss GI, Katona PG, and Chizeck HJ.** Adaptive multivariable drug delivery: control of arterial pressure and cardiac output in anesthetized dogs. *IEEE Trans Biomed Eng* 34: 617–623, 1987.
27. **Yu C, Roy RJ, Kaufman H, and Bequette BW.** Multiple-model adaptive predictive control of mean arterial pressure and cardiac output. *IEEE Trans Biomed Eng* 39: 765–778, 1992.

Available online at www.sciencedirect.com

SCIENCE DIRECT®

Life Sciences 78 (2006) 882 – 887

Life Sciences

www.elsevier.com/locate/lifescie

Vagal stimulation suppresses ischemia-induced myocardial interstitial norepinephrine release

Toru Kawada [a,*], Toji Yamazaki [b], Tsuyoshi Akiyama [b], Meihua Li [a], Hideto Ariumi [a], Hidezo Mori [b], Kenji Sunagawa [c], Masaru Sugimachi [a]

[a] *Department of Cardiovascular Dynamics, Advanced Medical Engineering Center, National Cardiovascular Center Research Institute, 5-7-1 Fujishirodai, Suita, Osaka 565-8565, Japan*

[b] *Department of Cardiac Physiology, National Cardiovascular Center Research Institute, Osaka 565-8565, Japan*

[c] *Department of Cardiovascular Medicine, Graduate School of Medical Sciences, Kyushu University, Fukuoka 812-8582, Japan*

Received 30 November 2004; accepted 31 May 2005

Abstract

Although electrical vagal stimulation exerts beneficial effects on the ischemic heart such as an antiarrhythmic effect, whether it modulates norepinephrine (NE) and acetylcholine (ACh) releases in the ischemic myocardium remains unknown. To clarify the neural modulation in the ischemic region during vagal stimulation, we examined ischemia-induced NE and ACh releases in anesthetized and vagotomized cats. In a control group (VX, $n=8$), occlusion of the left anterior descending coronary artery increased myocardial interstitial NE level from 0.46±0.09 to 83.2±17.6 nM at 30–45 min of ischemia (mean±SE). Vagal stimulation at 5 Hz (VS, $n=8$) decreased heart rate by approximately 80 beats/min during the ischemic period and suppressed the NE release to 24.4±10.6 nM ($P<0.05$ from the VX group). Fixed-rate ventricular pacing (VSP, $n=8$) abolished this vagally mediated suppression of ischemia-induced NE release. The vagal stimulation augmented ischemia-induced ACh release at 0–15 min of ischemia (VX: 11.1±2.1 vs. VS: 20.7±3.9 nM, $P<0.05$). In the VSP group, the ACh release was not augmented. In conclusion, vagal stimulation suppressed the ischemia-induced NE release and augmented the initial increase in the ACh level. These modulations of NE and ACh levels in the ischemic myocardium may contribute to the beneficial effects of vagal stimulation on the heart during acute myocardial ischemia.

Keywords: Acetylcholine; Coronary occlusion; Ventricular pacing

Introduction

Acute myocardial ischemia disrupts normal neural regulation of the heart (Armour, 1999). During prolonged ischemia, myocardial interstitial norepinephrine (NE) and acetylcholine (ACh) levels are increased in the ischemic region via local releasing mechanisms independent of efferent autonomic activities (Schömig et al., 1987; Lameris et al., 2000; Kawada et al., 2000, 2001). The excess NE release is thought to aggravate ischemic injury to the myocardium (Schömig et al., 1987). On the other hand, vagal stimulation exerts antiarrhythmic effects in the early phase of acute myocardial ischemia (Rosenshtraukh et al., 1994; Vanoli et al., 1991). A recent study from our laboratory demonstrated that vagal stimulation improved the survival rate of chronic heart failure after myocardial infarction in rats (Li et al., 2004), suggesting a long-term ameliorative effect of direct neural interventions against certain heart diseases.

With respect to electrical stimulation of the vagus, whether it alters myocardial interstitial NE and ACh levels in the ischemic region during acute myocardial ischemia remains unknown. To test the hypothesis that vagal stimulation increases the ACh level and suppresses the NE level in the ischemic region, we measured myocardial interstitial NE and ACh levels during acute myocardial ischemia in anesthetized cats using a cardiac microdialysis technique (Akiyama et al., 1991, 1994; Yamazaki et al., 1997). Effects of vagal stimulation were examined with or without fixed-rate ventricular pacing.

* Corresponding author. Tel.: +81 6 6833 5012x2427; fax: +81 6 6835 5403.
E-mail address: torukawa@res.ncvc.go.jp (T. Kawada).

0024-3205/$ - see front matter © 2005 Elsevier Inc. All rights reserved.
doi:10.1016/j.lfs.2005.05.087

Materials and methods

This investigation conforms with the *Guide for the Care and Use of Laboratory Animals* published by the US National Institutes of Health (NIH Publication No. 85-23, revised 1996).

Surgical preparation

Twenty-four adult cats weighing from 2.2 to 3.8 kg were anesthetized by an intraperitoneal injection of pentobarbital sodium (30–35 mg/kg) and ventilated mechanically with room air mixed with oxygen. The depth of anesthesia was maintained with a continuous intravenous infusion of pentobarbital sodium (1–2 mg kg^{-1} h^{-1}) through a catheter inserted from the right femoral vein to the inferior vena cava. Systemic arterial pressure (AP) was monitored from a catheter inserted from the right femoral artery into the abdominal aorta. Heart rate (HR) was determined from an electrocardiogram using a cardiotachometer. Esophageal temperature of the animal was measured using a thermometer (CTM-303, TERUMO, Japan) and was maintained at around 37 °C using a heated pad and a lamp.

Bilateral vagal nerves were sectioned through a midline cervical incision. With the animal in the lateral position, the left fifth and sixth ribs were resected to expose the heart. A dialysis probe was implanted, using a fine guiding needle, into the anterolateral free wall of the left ventricle perfused by the left anterior descending coronary artery (LAD). A 3-0 silk suture was passed around the LAD just distal to the first diagonal branch for later coronary occlusion. When an experimental protocol required electrical stimulation of the vagal efferent nerves, bipolar platinum electrodes were attached to the cardiac end of sectioned vagal nerves bilaterally. The nerves and electrodes were covered with warmed mineral oil for insulation. When an experimental protocol required cardiac pacing, bipolar stainless-steel wire electrodes were sutured at the left ventricular apex away from the implanted dialysis probe. Heparin sodium (100 U/kg) was administered intravenously to prevent blood coagulation.

In additional four anesthetized cats, the left ventricle was implanted with a dialysis probe and a pair of pacing electrodes to examine the effects of left ventricular pacing alone on the myocardial interstitial NE levels. The dialysis probe and pacing leads were placed in the same manner as described in the previous paragraph.

At the end of the experiment, the experimental animals were killed with an overdose of pentobarbital sodium. Postmortem examination confirmed that the dialysis probe had been implanted within the left ventricular myocardium.

Dialysis technique

The materials and properties of the dialysis probe have been previously described (Akiyama et al., 1991, 1994). Briefly, we designed a transverse dialysis probe. A dialysis fiber (13 mm length, 310 μm O.D., 200 μm I.D.; PAN-1200, 50,000 molecular weight cutoff, Asahi Chemical, Japan) was glued at both ends to polyethylene tubes (25 cm length, 500 μm O.D., 200 μm I.D.). The dialysis probe was perfused at a rate of 2 μl/min with Ringer solution containing the cholinesterase inhibitor eserine (100 μM). Dialysate sampling was initiated 2 h after implanting the dialysis probe, when the dialysate concentrations of NE and ACh had reached steady states (Akiyama et al., 1991, 1994). The actual dialysate sampling lagged behind a given collection period by 5 min taking into account the dead space volume between the dialysis membrane and the sample tube. Dialysate concentrations of NE and ACh were measured separately by high performance liquid chromatography with electrochemical detection (DTA-300, Eicom, Japan). Details of the NE and ACh measurements have been previously described (Akiyama et al., 1991, 1994).

Protocols

Protocol 1 (VX, n = 8)

As a control experiment, we measured ischemia-induced NE and ACh releases during 60-min LAD occlusion in vagotomized animals. After collecting a 15-min baseline dialysate sample, we occluded the LAD for 60 min and collected four consecutive 15-min dialysate samples during acute myocardial ischemia. We then loosened the LAD snare and collected a 15-min dialysate sample during reperfusion.

Protocol 2 (VS, n = 8)

We examined the effects of vagal stimulation on ischemia-induced NE and ACh releases. To avoid possible preconditioning mimetic effects of ACh released by vagal stimulation (Przyklenk and Kloner, 1995; Kawada et al., 2002a), we initiated the bilateral vagal stimulation (5 Hz, 1 ms in pulse duration and 10 V in pulse amplitude) at the onset of LAD occlusion. The vagal stimulation continued for the 60-min ischemic period and the 15-min reperfusion period.

Protocol 3 (VSP, n = 8)

To eliminate the effects of bradycardia associated with vagal stimulation, we performed vagal stimulation under fixed-rate pacing conditions. We initiated the bilateral vagal stimulation (5 Hz, 1 ms in pulse duration and 10 V in pulse amplitude) and paced the heart from the onset of LAD occlusion to the conclusion of the experimental period. The ventricular pacing rate was set close to the HR recorded immediately before the LAD occlusion.

Supplemental protocol (n = 4)

To examine the effects of left ventricular pacing on the myocardial interstitial NE levels, we collected 15-min dialysate samples under control conditions as well as under left ventricular pacing at 170 beats/min.

Statistical analysis

All data are presented as means ± SE values. In each group, the effects of LAD occlusion on dialysate concentrations of NE and ACh were examined using a repeated-measures analysis of

variance followed by a Dunnett test against respective baseline concentrations. Because the variance of NE data was very large and increased with mean, the NE data were compared after the logarithmic transform (Snedecor and Cochran, 1989). Differences were considered significant at $P<0.05$. To examine the effects of vagal stimulation with or without the ventricular pacing, dialysate concentrations of NE and ACh were compared among the three groups at each corresponding time period using one-way analysis of variance followed by a Student–Newman–Keuls test for all pairwise comparisons (Glantz, 2002). The NE data were compared after the logarithmic transform. Differences were considered significant at $P<0.05$. Heart rate and mean AP were determined immediately before the coronary occlusion (designated as time 0), after 5, 10, 15, 30, 45, and 60 min of the occlusion, and after 15 min of reperfusion. One-way analysis of variance followed by a Student–Newman–Keuls test was also applied to compare HR and mean AP among the three groups at each time point.

Results

Fig. 1 depicts LAD occlusion-induced myocardial interstitial NE accumulation within the ischemic zone. The inset shows the NE levels during baseline conditions in a magnified ordinate. In the VX group, LAD occlusion increased the NE level approximately 200 fold compared to the baseline level at 45–60 min. This occlusion-induced NE accumulation was significantly suppressed in the VS group compared with the VX group in 15–30, 30–45, and 45–60 min time periods. The difference between the VS and VX groups did not reach statistical significance at the reperfusion period. In the VSP group, in which HR was kept constant, vagal stimulation did not attenuate the occlusion-induced NE accumulation. In the supplemental protocol, the baseline myocardial interstitial NE level was 0.17±0.01 nM. The NE level during ventricular pacing at 170 beats/min was 0.21±0.09 nM.

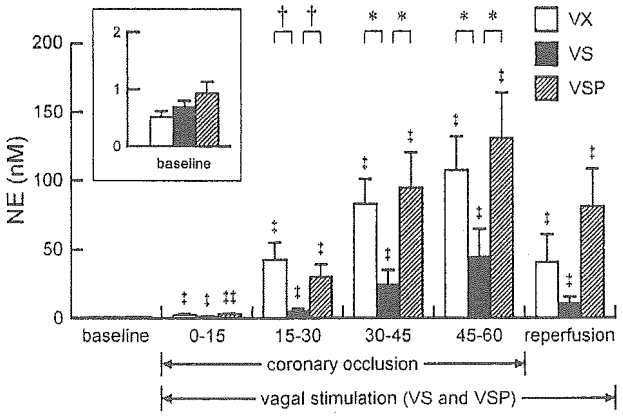

Fig. 1. Coronary occlusion-induced norepinephrine (NE) accumulation in the ischemic myocardium. VX: vagotomy, VS: vagal stimulation, VSP: vagal stimulation with ventricular pacing. The inset shows the baseline conditions with a magnified ordinate. Data are means±SE. $^{\ddagger}P<0.01$ and $^{\ddagger\ddagger}P<0.05$ from the corresponding baseline value in each group. $^{\dagger}P<0.01$ and $^{*}P<0.05$ by all pairwise comparisons among the three groups.

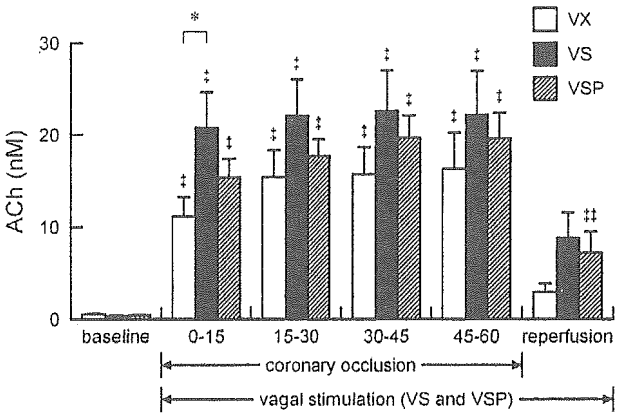

Fig. 2. Coronary occlusion-induced acetylcholine (ACh) accumulation in the ischemic myocardium. Data are means±SE. $^{\ddagger}P<0.01$ and $^{\ddagger\ddagger}P<0.05$ from the corresponding baseline value in each group. $^{*}P<0.05$ by all pairwise comparisons among the three groups.

Fig. 2 shows LAD occlusion-induced myocardial interstitial ACh accumulation within the ischemic zone. In the VX group, LAD occlusion increased the ACh level approximately 20 times higher than the baseline level at 45–60 min. The ACh level at 0–15 min was significantly higher in the VS than the VX group. For the rest of the ischemic period and reperfusion period, the differences between the VS and VX groups were not significant. The ACh levels in the VSP group did not differ from the VX group for any of the sampling periods.

Fig. 3 summarizes changes in HR and mean AP. In the VS group, HR was decreased by approximately 80 beats/min compared with the VX group at 5 min of coronary occlusion. The HR decrease continued for the rest of the ischemic period and reperfusion period. In the VSP group, HR was kept close to the preocclusion level, and it did not differ from the VX group

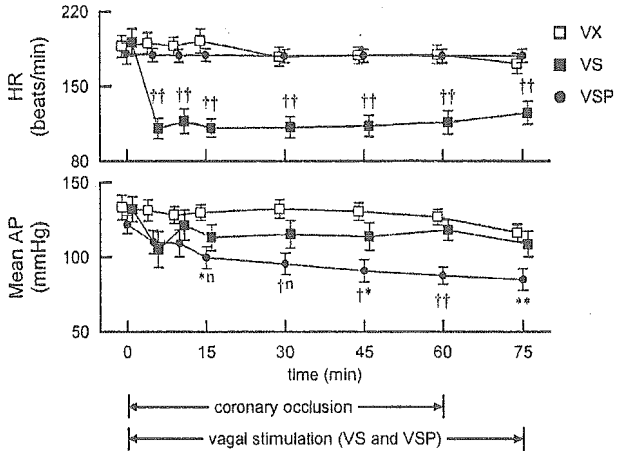

Fig. 3. Time courses of heart rate (HR) and mean arterial pressure (AP) during 60-min ischemia and 15-min reperfusion. The baseline values obtained just before coronary occlusion are plotted at time 0. Data points for VX and VSP groups are slightly displaced along the time axis for better view of overlapping points. Data are means±SE. In the HR data, †† represents statistical significance of $P<0.01$ from both the VX and VSP groups by all pairwise comparisons. In the AP data, when two characters are added to the VSP data point, the first and second characters represent the statistical significance from VX and VS groups, respectively. *, †, and n designate $P<0.05$, $P<0.01$, and "not significant", respectively.

for all the time points. Mean AP did not differ statistically between VX and VS groups. Mean AP in the VSP group progressively decreased and became significantly lower than the VX group after 15 min of the ischemic period. Mean AP in the VSP group was also significantly lower than the VS group after 45 min of the ischemic period.

Discussion

We have shown that electrical vagal stimulation suppressed ischemia-induced NE release and enhanced an initial increase in the ACh levels in the ischemic myocardium. Fixed-rate pacing abolished the suppression of ischemia-induced NE release by vagal stimulation in the present experimental settings.

Effects of vagal stimulation on ischemia-induced NE release

Several mechanisms can be put forward to explain the suppression of ischemia-induced myocardial interstitial NE release by vagal stimulation. First, activation of presynaptic muscarinic receptors on the sympathetic nerve endings inhibits the exocytotic NE release under normal physiological conditions (Levy and Blattberg, 1976). However, the presynaptic inhibition is unlikely the mechanism underlying the vagally mediated suppression of the ischemia-induced NE release because of the following reasons. Although the exocytotic release mechanism participates in the ischemia-induced NE release within the first 20 min of ischemia, the non-exocytotic release mechanism becomes predominant as the ischemic period is prolonged (Akiyama and Yamazaki, 1999). Myocardial ischemia gradually depletes ATP in the ischemic region including sympathetic nerve terminals, which leads to accumulation of axoplasmic NE and reduction of normal Na^+gradient across the plasma membrane in the sympathetic nerve terminals. The NE uptake transporter on the sympathetic nerve terminals, driven by the Na^+gradient, is then reversed, evoking non-exocytotic NE release (Schwartz, 2000). Therefore, the presynaptic inhibition of exocytotic NE release might contribute little to the suppression of ischemia-induced NE release during prolonged ischemia. Furthermore, the presynaptic inhibition of exocytotic NE release becomes less effective during the ischemic insult (Du et al., 1990; Haunstetter et al., 1994). The fact that the ischemia-induced NE release did not differ between the VSP and VX groups is also in opposition to the presynaptic inhibition as a chief mechanism underlying the vagally mediated suppression of ischemia-induced NE release (Fig. 1). Although left ventricular pacing could have affected myocardial interstitial NE levels, the results of the supplemental protocol indicates that changes in the NE levels by ventricular pacing might be negligibly small compared to the ischemia-induced NE release.

Second, the suppression of ischemia-induced NE release by vagal stimulation may be related to myocardial protection via direct vasodiation of the coronary artery. The coronary dilation may enhance collateral flow in the ischemic region and protect against myocardial deterioration evoked by ischemia. Both ACh and vasoactive intestinal polypeptide (VIP) are known to exert direct coronary dilation (Feliciano and Henning, 1998; Gross et al., 1981; Henning and Sawmiller, 2001). VIP is colocalized with ACh in the postganglionic vagal fibers and is released by high-frequency (20 Hz) vagal stimulation. VIP may interact with NE transport or exocytosis like nociceptin (Yamazaki et al., 2001). However, fixed-rate pacing abolished the ability of vagal stimulation to suppress the ischemia-induced NE release. Hence the direct coronary vasodilation and/or interaction with the sympathetic system via VIP might have played little role in suppressing ischemia-induced NE release in the present experimental settings. Another factor that should be taken into account is that the relatively low-frequency (5 Hz) stimulation might have limited the amount of VIP release from the vagal nerve endings.

Third, HR is one of the most important determinants of myocardial oxygen consumption (Mohrman and Heller, 1997). In the present study, HR in the VS group decreased to approximately 60% that of the VX group during the ischemic period (Fig. 3), which slowed the energy consumption of the myocardium. Bradycardia might also decrease ventricular contractility via a force-frequency mechanism (Maughan et al., 1985). In addition, bradycardia may increase coronary perfusion via prolongation of diastolic interval (Buck et al., 1981). These factors slowed energy consumption in the ischemic region including sympathetic nerve terminals, delaying the time course for non-exocytotic NE release. The prevention of excess NE would further reduce myocardial oxygen consumption and decelerate the progression of ischemic injury (Suga et al., 1983). The ischemia-induced NE release did not differ between the VSP and VX groups despite the lower mean AP in the VSP compared with the VX group. Although lowering AP might decrease afterload of the ventricle and reduce energy consumption, the beneficial effect of afterload reduction might have been masked in the VSP group due to inefficient cardiac pumping function associated with asynchrony between sinus rate and ventricular rate. Proper atrioventricular conduction time contributes to the ventricular filling (Meisner et al., 1985). In the VSP group, the sinus rate was reduced by vagal stimulation whereas the ventricular rate was maintained by fixed-rate pacing. Dissociation of the sinus rate and ventricular rate might have impaired the ventricular filling to a variable extent, resulting in a progressive reduction in AP.

Finally, the vagal stimulation decreases ventricular contractile force against sympathetic activation via the direct projections to the ventricle (Nakayama et al., 2001). This mechanism might have also contributed to the reduction of the myocardial oxygen consumption and slowed the progression of ischemic injury in the VS group. However, the ventricular pacing canceled the protective effects in the VSP group, possibly by the adverse influences discussed in the previous paragraph. Further studies are required to isolate the factor(s) most important for the suppression of ischemia-induced NE release by the vagal stimulation.

Effects of vagal stimulation on ischemia-induced ACh release

In contrast to the suppressive effect of NE release, vagal nerve stimulation can exert two opposing influences on ACh release in the ischemic myocardium. The nerve stimulation itself induces exocytotic ACh release from nerve endings. Acute myocardial ischemia impairs conduction of the nerves traversing in the ischemic region (Barber et al., 1983; Inoue and Zipes, 1988; Martins et al., 1989). Acute myocardial ischemia also impairs the exocytotic ACh release in the postischemic myocardium (Kawada et al., 2002b). On the other hand, acute myocardial ischemia causes myocardial ACh release in the ischemic region via a local release mechanism independent of efferent nerve activity (Kawada et al., 2000). Hence, the amount of ACh release was net effects of ACh release evoked by nerve stimulation and ischemia; vagally mediated protection against ischemic injury should augment the former and attenuate the latter.

Although vagal stimulation augmented myocardial interstitial ACh release during the 0–15 min period of coronary occlusion in the VS group than in the VX group, the initial enhancement was not observed in the VSP group. One possible mechanism for the difference in the initial ACh release between the VS and VSP groups is that the progression of ischemia in the VSP group relative to the VS group impaired the vagal nerve conduction in the ischemic region, reducing the exocytotic ACh release. The other possible mechanism is that the high levels of NE might have attenuated the stimulation-induced ACh release from the vagal nerve endings via α-adrenergic mechanisms (Akiyama and Yamazaki, 2000).

There are several limitations to the present study. First, we avoided large myocardial ischemia by occluding LAD just distal to the first diagonal branch. Accordingly, the incidence of lethal ventricular arrhythmia was too low to draw any conclusion as to the effects of vagal stimulation on the arrhythmogenesis. Further studies with larger myocardial ischemia are clearly required to examine the effects of vagal stimulation on the incidence of lethal ventricular arrhythmia in relation to the observed NE and/or ACh levels in the ischemic myocardium. Second, plasma catecolamine levels might have been increased during the LAD occlusion, which might affect HR and cardiac function in the non-ischemic region. Although changes in plasma catecholamine levels may play significant roles in determining systemic hemodynamics, the ischemic region was only poorly perfused. Accordingly, direct effects of plasma catecholamines on the myocardial interstitial NE and ACh levels in the ischemic region might have been limited in the present study.

Conclusion

Electrical vagal stimulation suppressed ischemia-induced NE release in the ischemic myocardium in anesthetized cats. The vagal stimulation augmented ischemia-induced ACh release at the 0–15 min period of ischemia. Although acute myocardial ischemia causes myocardial NE and ACh releases independent of efferent nerve activity, the vagal stimulation was able to modulate both NE and ACh levels in the ischemic region. The suppression of NE release and augmentation of initial ACh release in the ischemic myocardium by vagal stimulation may reduce the ischemic injury to the heart. The direct neural intervention could be a new modality of medical engineering to cope with ischemic heart diseases.

Acknowledgments

This study was supported by Health and Labour Sciences Research Grant for Research on Advanced Medical Technology (H14-Nano-002) from the Ministry of Health Labour and Welfare of Japan, by Grant-in-Aid for Scientific Research (C-15590786) from the Ministry of Education, Science, Sports and Culture of Japan, and by the Program for Promotion of Fundamental Studies in Health Science from the Organization for Pharmaceutical Safety and Research.

References

Akiyama, T., Yamazaki, T., 1999. Norepinephrine release from cardiac sympathetic nerve endings in the in vivo ischemic region. Journal of Cardiovascular Pharmacology 34, S11–S14.

Akiyama, T., Yamazaki, T., 2000. Adrenergic inhibition of endogenous acetylcholine release on postganglionic cardiac vagal nerve terminals. Cardiovascular Research 46, 531–538.

Akiyama, T., Yamazaki, T., Ninomiya, I., 1991. In vivo monitoring of myocardial interstitial norepinephrine by dialysis technique. American Journal of Physiology. Heart and Circulatory Physiology 261, H1643–H1647.

Akiyama, T., Yamazaki, T., Ninomiya, I., 1994. In vivo detection of endogenous acetylcholine release in cat ventricles. American Journal of Physiology. Heart and Circulatory Physiology 266, H854–H860.

Armour, J.A., 1999. Myocardial ischaemia and the cardiac nervous system. Cardiovascular Research 41, 41–54.

Barber, M.J., Mueller, T.M., Henry, D.P., Felten, S.Y., Zipes, D.P., 1983. Transmural myocardial infarction in the dog produces sympathectomy in noninfarcted myocardium. Circulation 67, 787–796.

Buck, J.D., Warltier, D.C., Hardman, H.F., Gross, G.J., 1981. Effects of sotalol and vagal stimulation on ischemic myocardial blood flow distribution in the canine heart. Journal of Pharmacological and Experimental Therapeutics 216, 347–351.

Du, X.J., Dart, A.M., Riemersma, R.A., Oliver, M.F., 1990. Failure of the cholinergic modulation of norepinephrine release during acute myocardial ischemia in the rat. Circulation Research 66, 950–956.

Feliciano, L., Henning, R.J., 1998. Vagal nerve stimulation releases vasoactive intestinal peptide which significantly increases coronary artery blood flow. Cardiovascular Research 40, 45–55.

Glantz, S.A., 2002. Primer of Biostatistics, 5th ed. McGraw-Hill, New York.

Gross, G.J., Buck, J.D., Warltier, D.C., 1981. Transmural distribution of blood flow during activation of coronary muscarinic receptors. American Journal of Physiology. Heart and Circulatory Physiology 240, H941–H946.

Haunstetter, A., Haass, M., Yi, X., Krüger, C., Kübler, W., 1994. Muscarinic inhibition of cardiac norepinephrine and neuropeptide Y release during ischemia and reperfusion. American Journal of Physiology. Regulatory, Integrative and Comparative Physiology 267, R1552–R1558.

Henning, R.J., Sawmiller, D.R., 2001. Vasoactive intestinal peptide: cardiovascular effects. Cardiovascular Research 49, 27–37.

Inoue, H.,. Zipes, D.P., 1988. Time course of denervation of efferent sympathetic and vagal nerves after occlusion of the coronary artery in the canine heart. Circulation Research 62, 1111–1120.

Kawada, T., Yamazaki, T., Akiyama, T., Sato, T., Shishido, T., Inagaki, M., Takaki, H., Sugimachi, M., Sunagawa, K., 2000. Differential acetylcholine release mechanisms in the ischemic and non-ischemic myocardium. Journal of Molecular and Cellular Cardiology 32, 405–414.

Kawada, T., Yamazaki, T., Akiyama, T., Inagaki, M., Shishido, T., Zheng, C., Yanagiya, Y., Sugimachi, M., Sunagawa, K., 2001. Vagosympathetic interactions in ischemia-induced myocardial norepinephrine and acetylcholine release. American Journal of Physiology. Heart and Circulatory Physiology 280, H216–H221.

Kawada, T., Yamazaki, T., Akiyama, T., Mori, H., Inagaki, M., Shishido, T., Takaki, H., Sugimachi, M., Sunagawa, K., 2002. Effects of brief ischaemia on myocardial acetylcholine and noradrenaline levels in anaesthetized cats. Autonomic Neuroscience 95, 37–42.

Kawada, T., Yamazaki, T., Akiyama, T., Mori, H., Uemura, K., Miyamoto, T., Sugimachi, M., Sunagawa, K., 2002. Disruption of vagal efferent axon and nerve terminal function in the postischemic myocardium. American Journal of Physiology. Heart and Circulatory Physiology 283, H2687–H2691.

Lameris, T.W., de Zeeuw, Sandra, Alberts, G., Boomsma, F., Duncker, D.J., Verdouw, P.D., Veld, A.J., van den Meiracker, A.H., 2000. Time course and mechanism of myocardial catecholamine release during transient ischemia in vivo. Circulation 101, 2645–2650.

Levy, M.N., Blattberg, B., 1976. Effect of vagal stimulation on the overflow of norepinephrine into the coronary sinus during cardiac sympathetic nerve stimulation in the dog. Circulation Research 38, 81–84.

Li, M., Zheng, C., Sato, T., Kawada, T., Sugimachi, M., Sunagawa, K., 2004. Vagal nerve stimulation markedly improves long-term survival after chronic heart failure in rats. Circulation 109, 120–124.

Martins, J.B., Lewis, R., Wendt, D., Lund, D.D., Schmid, P.G., 1989. Subendocardial infarction produces epicardial parasympathetic denervation in canine left ventricle. American Journal of Physiology. Heart and Circulatory Physiology 256, H859–H866.

Maughan, W.L., Sunagawa, K., Burkhoff, D., Graves, W.L. Jr., Hunter, W.C., Sagawa, K., 1985. Effect of heart rate on the canine end-systolic pressure–volume relationship. Circulation 72, 654–659.

Meisner, J.S., McQueen, D.M., Ishida, Y., Vetter, H.O., Bortolotti, U., Strom, J.A., Frater, R.W.M., Peskin, C.S., Yellin, E.L., 1985. Effects of timing of atrial systole on LV filling and mitral valve closure: computer and dog studies. American Journal of Physiology. Heart and Circulatory Physiology 249, H604–H619.

Mohrman, D.E., Heller, L.J., 1997. Cardiovascular Physiology, 4th ed. McGraw-Hill, New York, pp. 47–69.

Nakayama, Y., Miyano, H., Shishido, T., Inagaki, M., Kawada, T., Sugimachi, M., Sunagawa, K., 2001. Heart rate-independent vagal effect on end-systolic elastance of the canine left ventricule under various levels of sympathetic tone. Circulation 104, 2277–2279.

Przyklenk, K., Kloner, R.A., 1995. Low-dose i.v. acetylcholine acts as a "preconditioning-mimetic" in the canine model. Journal of Cardiac Surgery 10, 389–395.

Rosenshtraukh, L., Danilo Jr., P., Anyukhovsky, E.P., Steinberg, S.F., Rybin, V., Brittain-Valenti, K., Molina-Viamonte, V., Rosen, M.R., 1994. Mechanisms for vagal modulation of ventricular repolarization and of coronary occlusion-induced lethal arrhythmias in cats. Circulation Research 75, 722–732.

Schömig, A., Fischer, S., Kurz, T., Richardt, G., Schömig, E., 1987. Nonexocytotic release of endogenous noradrenaline in the ischemic and anoxic rat heart: mechanism and metabolic requirements. Circulation Research 60, 194–205.

Schwartz, J.H., 2000. Neurotransmitters. In: Kandel, E.R., Schwartz, J.H., Jessell, T.M. (Eds.), Principles of Neural Science, 4th ed. McGraw-Hill, New York, pp. 280–297.

Snedecor, G.W., Cochran, W.G., 1989. Statistical Methods, 8th ed. Iowa State, Iowa, pp. 290–291.

Suga, H., Hisano, R., Goto, Y., Yamada, O., Igarashi, Y., 1983. Effect of positive inotropic agents on the relation between oxygen consumption and systolic pressure volume area in canine left ventricle. Circulation Research 53, 306–318.

Vanoli, E., De Ferrari, G.M., Stramba-Badiale, M., Hull Jr., S.S., Foreman, R.D., Schwartz, P.J., 1991. Vagal stimulation and prevention of sudden death in conscious dogs with a healed myocardial infarction. Circulation Research 68, 1471–1481.

Yamazaki, T., Akiyama, T., Kitagawa, H., Takauchi, Y., Kawada, T., Sunagawa, K., 1997. A new, concise dialysis approach to assessment of cardiac sympathetic nerve terminal abnormalities. American Journal of Physiology. Heart and Circulatory Physiology 272, H1182–H1187.

Yamazaki, T., Akiyama, T., Mori, H., 2001. Effects of nociceptin on cardiac norepinephrine and acetylcholine release evoked by ouabain. Brain Research 904, 153–156.

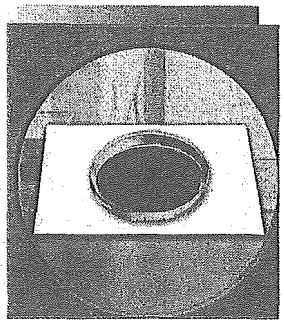

Bionic Cardiovascular Medicine

Functional Replacement of Native Cardiovascular Regulation and the Correction of Its Abnormality

BY MASARU SUGIMACHI
AND KENJI SUNAGAWA

We have developed a novel, bionic therapeutic strategy to treat various incurable cardiovascular diseases. The bionic therapeutic strategy comprises a collection of methods to treat various diseases by replacing the native regulatory function or by correcting the abnormal native function with intelligent electronic devices. We have succeeded in decoding the heart rate from the sympathetic nervous system, encoding pressor information and delivering it via nervous stimulation sequence, and improving the survival of animals with chronic heart failure by the correction of the abnormal cardiovascular regulatory function.

Bionic Cardiovascular Medicine

The term *bionic therapeutic strategy* denotes a collection of methods used to treat various diseases by replacing the native regulatory system with intelligent electronic devices [Figure 1(a)]. This strategy allows treatment of various cardiovascular diseases by compensating the deficiencies of the native cardiovascular regulatory system caused by diseases. If the electronic device can mimic native regulatory function, then it can also regulate the cardiovascular system and operate as if it were the native system. To achieve this goal, one has to interface the device with the autonomic nervous system. Depending on whether the neural interface is on the afferent or efferent side of the device, the device is able to either listen to the voices of the autonomic nerves or drive the autonomic nerves to execute appropriate cardiovascular control.

In one of our studies, we have tried to decipher the message from the brain by decoding the efferent neural activities. In our specific study detailed in the following, this approach effectively replaces the neural control of heart rate. This framework proved useful in the development of a neural-regulated cardiac pacemaker [1]. The pacemaker is able to adjust the heart rate as if it were regulated by the native sympathetic nervous system.

In another study, we have developed techniques to drive the autonomic nervous system by encoding information for cardiovascular control and delivering it via the neural stimulation sequence. This allows us to replace part of the medullary regulatory function; in other words, to create the brain function. Using this framework, we were able to replace the medullary vasomotor center and restore the normal pressure-stabilizing function of the brain [2], [3].

In yet another study, the bionic therapeutic strategy was able to correct the abnormal regulatory function accompanying some diseases [Figure 1(b)]. This correction proved to be effective in improving the survival of animals with chronic heart failure [4]. We have also demonstrated that altering native function rather than mimicking it has beneficial effects on survival in chronic heart failure. In this case, the electronic device can augment brain function.

Functional Identification of the Cardiovascular System: White-Noise Method

Replacement of lost native function or correction of abnormal native function requires comprehensive identification of the normal cardiovascular regulatory system. For this purpose, we used the white-noise method, where white noise was imposed as the input to the system to be identified. The wideband nature of white-noise input allows estimation of the wideband system dynamic properties. In addition, we ensemble-averaged the input power and cross power to reduce the statistical variance [5]–[7].

As shown in Figure 2, both input, $x(t)$, and output, $y(t)$, signals are divided into multiple segments. These data are subjected to frequency analysis using a fast Fourier transform (FFT) algorithm, $X(f)$ and $Y(f)$. The calculated input power and cross power (between input and output signals) are ensemble-averaged across segments to reduce variance, $XX(f)$ and $YX(f)$. Finally, the transfer function $H(f)$ is obtained by dividing the ensembled cross power by the ensembled input power. The impulse response $h(t)$ is calculated by the inverse FFT of the transfer function.

Deciphering the Message from the Brain: Development of a Neural-Regulated Pacemaker

The cardiac pacemaker is an established device used to treat bradyarrhythmias. Development of the dual-chamber (DDD) pacemaker has improved the coordination between the electrical activity of the atria and ventricles. In patients with preserved atrial function, a DDD pacemaker allows changes in heart rate in response to exercise as well as psychological excitation. To treat patients who have lost atrial function, it is

 0739-5175/05/$20.00©2005IEEE

necessary to stimulate the atrium in a physiological manner. For this purpose, the rate-responsive (DDDR) pacemaker has been developed [8]. The DDDR pacemaker is designed to change heart rates in response to changes such as body temperature, acceleration, and electrocardiographic QT interval. Even with the rate-responsive pacemaker, however, the heart rate responses are still not quite physiological.

In animals and humans, heart rate is regulated by the autonomic (sympathetic and vagal) nervous system [9]–[11]. Since information on the true physiological target of heart rate control is contained within the autonomic nervous activity; deriving heart rate changes continuously from analysis of neural activity has made it possible to develop a truly physiological pacemaker; the neural-regulated pacemaker (Figure 3). In other words, the message from the brain can be deciphered by decoding the heart rate information from the efferent neural traffic. A neural-regulated pacemaker is then able to adjust heart rate as if it were regulated by the native sympathetic nervous system.

Figure 4 illustrates an example of our attempt to decode heart rate information from sympathetic nervous activity. We first examined the instantaneous relationship between nervous activity and heart rate [see time course Figure 4(a)]. A scatter plot of these two variables [Figure 4(c)] seems to show that they are not at all related.

To further investigate the relationship between nervous activity and heart rate, we identified the transfer function and the impulse response of the system. The results indicate that heart rate is dependent on not only the instantaneous nervous activity but also its history (Figure 5). Specifically, the impulse response $h(k)$ quantifies the effect of past nervous activity $NA(n-k)$ on heart rate $HR(n)$ at a point in time n.

Figure 4(b) provides an example of how the impulse response is used successfully to decode heart rate from current and past nervous activities. The estimated changes in heart

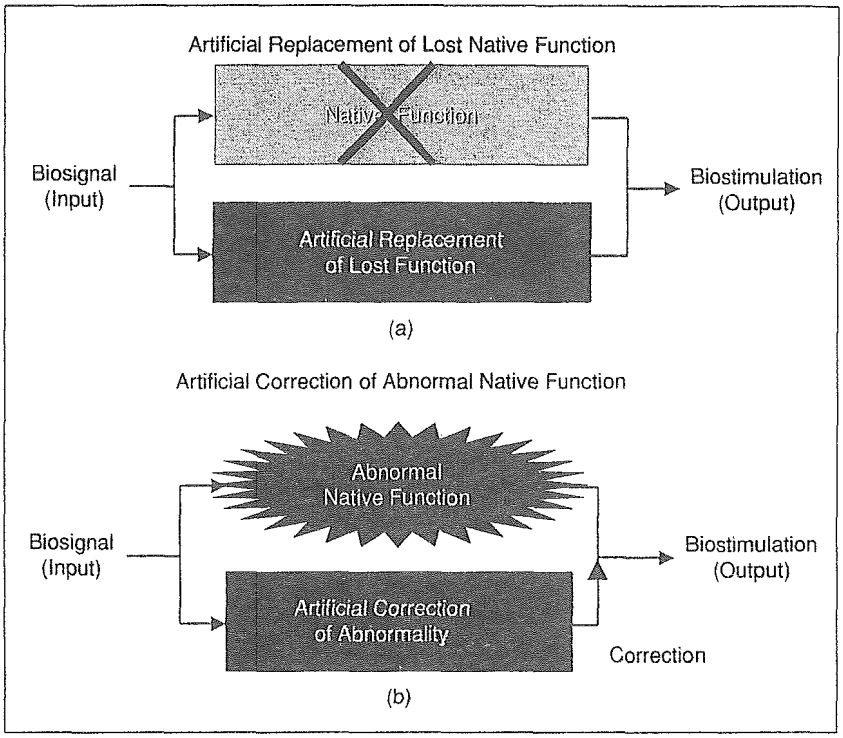

Fig. 1. Bionic medicine either replaces the lost native function or corrects the abnormal native function with the use of artificial devices.

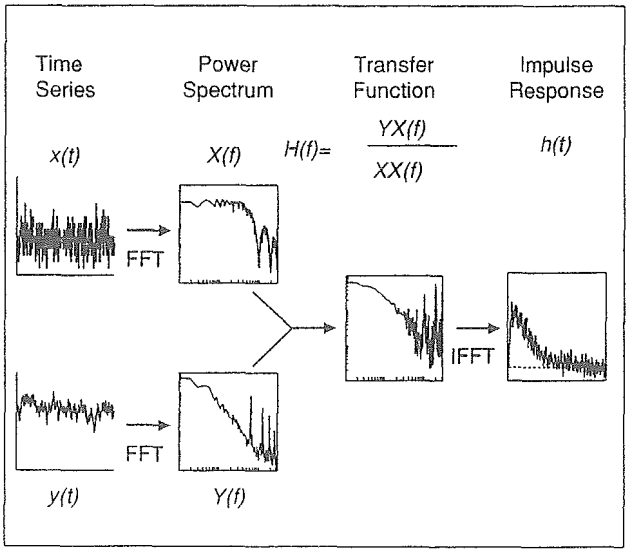

Fig. 2. Functional identification of the native regulatory system with the white-noise method. Transfer function and impulse response describe the comprehensive dynamic properties: *x(t)*, input; *y(t)*, output; *X(f)*, input spectrum; *Y(f)*, output spectrum; *XX(f)*, input power; *YX(f)*, cross power; *H(f)*, transfer function; *h(t)*, impulse response.

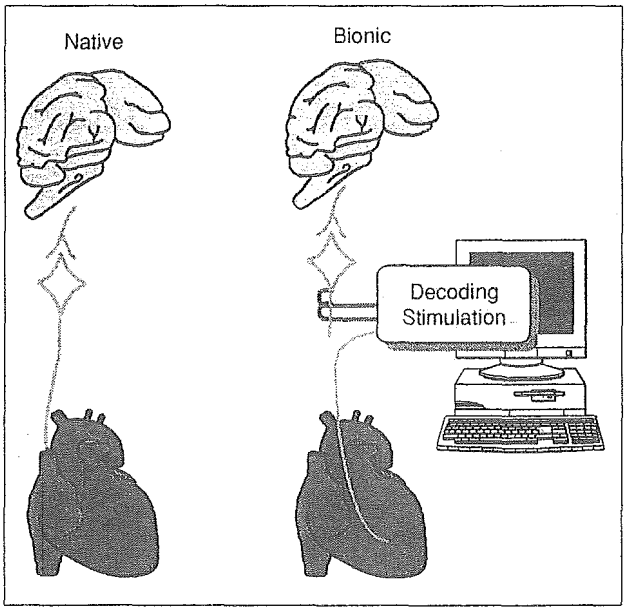

Fig. 3. Schematic presentation of the bionic (neural-regulated) pacemaker. By deciphering the message from the brain (decoding from the neural activity), one can reproduce the truly physiological changes in heart rate.

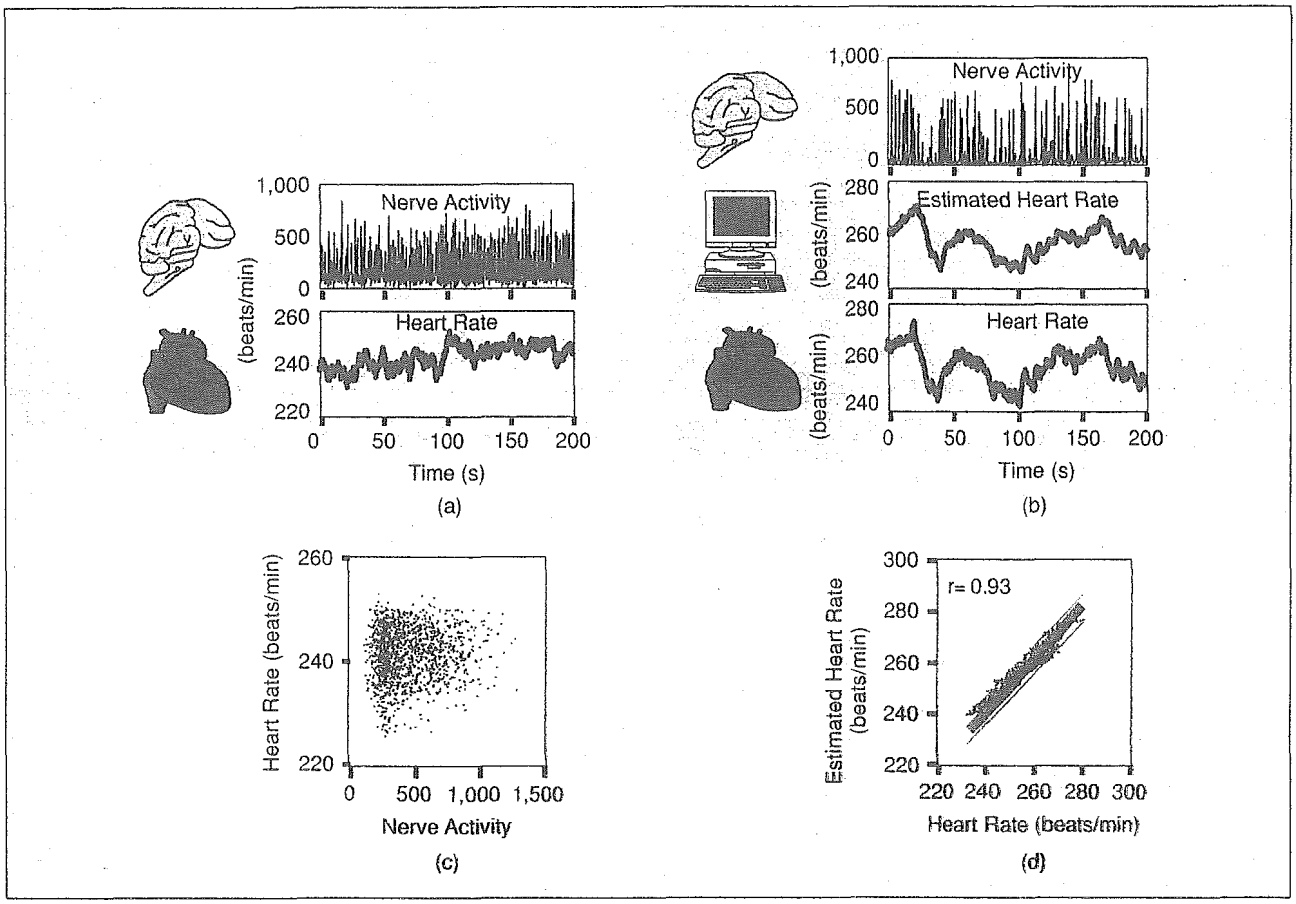

Fig. 4. An example showing how the decoding improves the estimation accuracy of the physiological changes in heart rate (modified from (1)).

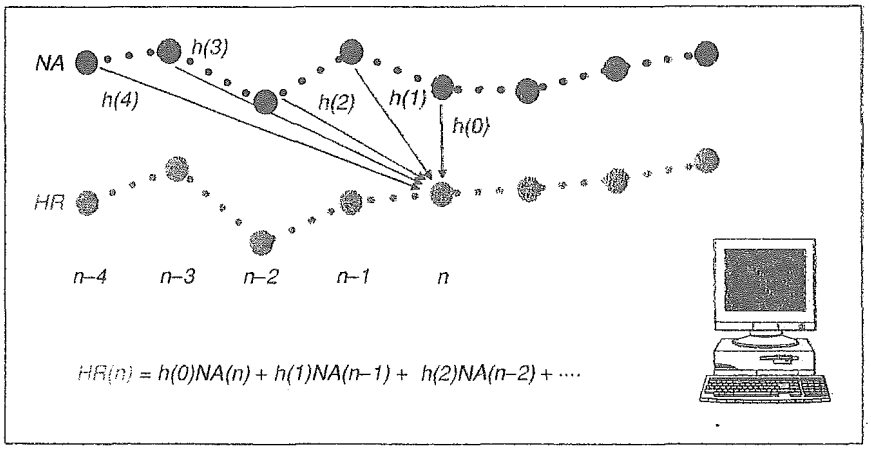

Fig. 5. Heart rate is determined not only by the instantaneous nervous activity, but also by its history. The impulse response, *h(k)*, represents how each past neural activity, *NA(n-k)*, affects the heart rate, *HR(n)*.

rate (time course) are shown to almost superimpose the measured changes [Figure 4(b)]. The accuracy of the estimation is further demonstrated by the scatter plot [Figure 4(d)]. In this particular example, the correlation coefficient was 0.93.

Accurate estimation of heart rate has also been achieved in other animals [1]. In eight anesthetized rabbits, the transfer function was approximated by a first-order, low-pass filter (corner frequency, 0.024 ± 0.013 Hz) with a lag time of 0.98 ± 0.09 s. The estimated heart rate correlated well with the measured heart rate, with correlation coefficients between 0.80 and 0.98. The standard error of the prediction was 1.2 ± 0.7% of the average heart rate examined, indicating that the heart rate estimation is sufficiently accurate for use in cardiac pacing. Thus, decoding instantaneous heart rate from sympathetic nervous activity is possible via impulse response analysis. This framework enables the development of a neural-regulated artificial pacemaker with a truly physiological heart rate control.

Creating the Brain: Development of Artificial Vasomotor Center

It is well known that animals and humans are equipped with baroreceptors (pressure sensors) in the walls of the carotid sinus and aortic arch. Information from these baroreceptors is used to stabilize blood pressure and maintain the homeostasis of the body. This pressure stabilizing system forms a negative feedback system, which is called the arterial baroreflex system. A decrease in blood pressure induces a pressor command at the vasomotor center located in the medulla. The pressor command increases pressure through a positive inotropic and chronotropic effect on the heart, and a vasoconstrictive effect on the blood vessels [12].

Patients lacking a functional vasomotor center in the brain suffer from severe orthostatic hypotension, and are often confined to bed [13]. They include patients with spinal cord injury and central degenerative diseases such as Shy-Drager syndrome. These patients lose consciousness during sitting and standing due to the severe hypotension attending these conditions, despite normal functions of the cardiovascular system and peripheral sympathetic nervous system. In fact, these patients suffer from hypertension in the supine position.

Blood pressure can be measured with artificial manometers (pressure sensors) such as semiconductor sensors. By feeding the blood pressure information into an electronic device that substitutes the nonfunctioning native vasomotor center, it is possible to drive the sympathetic nervous system (Figure 6). If the sympathetic nerve is appropriately stimulated to provide a sufficiently quick and stable feedback system, then the pressure-stabilizing function of the arterial baroreflex system can be restored.

One of the methods to achieve appropriate stimulation is to mimic the function of the native vasomotor center. If the mechanism of how the native vasomotor center drives the sympathetic nervous system in response to pressure changes is elucidated, then the feedback loop may be closed with sufficient speed and stability [14]–[17]. Since this treatment framework involves replacing a part of the brain function with an artificial device, it is called bionic treatment with electronic creation of brain function.

We first examined experimentally whether restoration of vasomotor center function is possible in anesthetized rats. We placed a catheter-tipped micromanometer in the aortic arch and implanted stimulation electrodes on the greater splanchnic nerve (celiac ganglion).

The encoding rule for the bionic brain (artificial vasomotor center) was determined by a white-noise approach in the following manner (Figure 7). We first estimated the open-loop dynamic properties of the native total baroreflex system. The dynamic properties, i.e., the transfer function (H_{NATIVE}), were obtained by analyzing the dynamic relationships between carotid sinus pressure (input) and blood pressure (output) after carotid sinus isolation and aortic denervation. We then determined the dynamic response of blood pressure (AoP) to electrical stimulation (STM) of the celiac ganglion ($H_{STM \rightarrow AoP}$: effector response). To match the dynamic properties of the total baroreflex response with the serially connected bionic brain and the effector response, we computed the dynamic property (encoding rule, H_{BIONIC}) of the bionic brain by $H_{NATIVE}/H_{STM \rightarrow AoP}$ and entered the encoding rule into the computer. The open-loop transfer function of the artificial vasomotor center was identified as a high-pass filter with a corner frequency of 0.1 Hz [2], [3], [18].

Figure 8 depicts an example of how functional replacement of the vasomotor center with the bionic brain restores the pressure stabilization after head-up tilt tests. The rat was subjected to a constant baroreflex input by carotid sinus isolation and aortic denervation. This procedure produced a "baroreflex failure" rat.

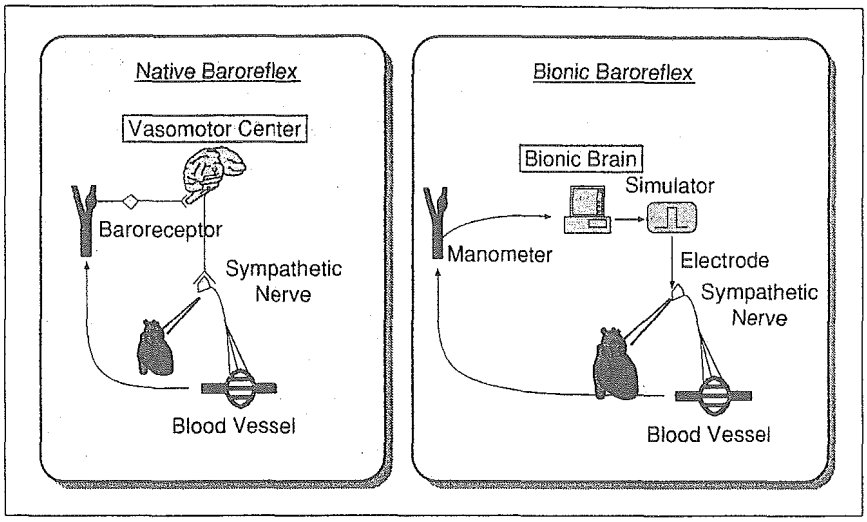

Fig. 6. Schematic presentation of the bionic baroreflex. The bionic brain (artificial vasomotor center) drives the sympathetic nerves in response to pressure perturbation. The encoding rule was obtained by mimicking the native vasomotor center. The bionic brain functionally replaces the vasomotor center, artificially creating the brain function (modified from (2)).

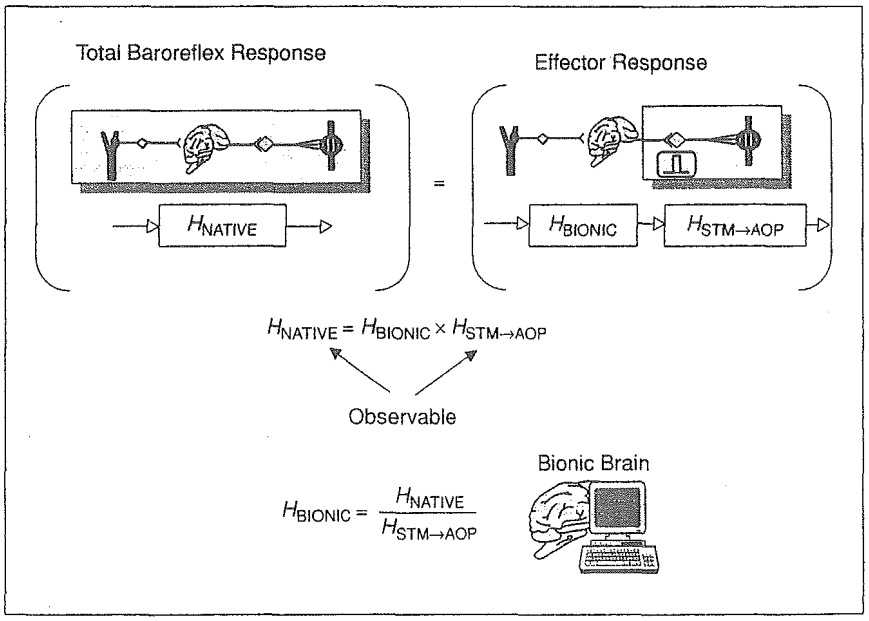

Fig. 7. Method to identify the dynamic properties of the bionic brain. H_{NATIVE}, total baroreflex properties; H_{BIONIC}, bionic brain (artificial vasomotor center) properties; $H_{STM \rightarrow AoP}$, effector properties; *STM*, electrical stimulation frequency; *AoP*, blood pressure (modified from (2)).

If the electronic device can mimic native regulatory function, then it can also regulate the cardiovascular system and operate as if it were the native system.

In a rat with normal baroreflex, a 90° head-up tilt decreases blood pressure by approximately 10 mmHg. When the "baroreflex failure" rat was tested, the head-up tilt drastically decreased blood pressure by approximately 50 mmHg. By activating the bionic baroreflex in the "baroreflex failure" rat, blood pressure did not decrease more than 10 mmHg.

Pressure stabilization provided by the bionic brain was verified in other experiments using rats [2], [3]. The pressure stabilization process was examined by two approaches. First, we evaluated the performance of the bionic brain in response to sudden local imposition of a pressure step on carotid sinus baroreceptors in 16 anesthetized rats [2]. Without the bionic brain, blood pressure fell rapidly by 49 ± 8 mmHg in 10 s. With the bionic brain online in real-time execution mode, blood pressure fell only by 22 ± 6 mmHg at the nadir and by 16 ± 5 mmHg at the plateau. These pressure changes were statistically indistinguishable from those of the native baroreflex system.

In ten other rats with baroreflex failure, we evaluated the performance of the bionic brain by the 90° head-up tilt tests [3]. Abrupt head-up tilt decreased blood pressure by 34 ± 6 mmHg in 2 s and by 52 ± 5 mmHg in 10 s. With real-time execution of the bionic brain, the pressure fall was only 21 ± 5 mmHg at 2 s and 15 ± 6 mmHg at 10 s after starting the head-up tilt. The pressure responses observed with the bionic brain in action were indistinguishable from those observed with a normal native baroreflex system.

From these data, we conclude that the bionic brain is able to restore the native baroreflex function in rats with baroreflex failure. Development of appropriate long-term manometry and an implantable neural stimulation system would provide a novel modality to treat incurable bed-ridden conditions such as Shy-Drager syndrome.

Surpassing the Native Brain: Bionic Treatment of Chronic Heart Failure

Bionic treatment so far, described as "deciphering the message of the brain" and "creating the brain function," operates by replacing the lost native function with artificial electronic devices. These devices operate as if they were native regulatory systems. However, in some pathological states, the native regulatory system acts in a detrimental fashion against recovery from the disease. Heart failure is perhaps the most well-known disease in which the native regulatory system is essential for the maintenance and progression of the disease [19]. In heart failure, there is a possibility that correction of the abnormal regulatory function may inhibit or slow the progression of the disease. If this treatment proves effective, it will open a possibility of yet another type of bionic treatment, which we designate "surpassing the native brain function." In earlier studies, diminished cardiac vagal activity and higher heart rate predict a high mortality of heart failure [20]. Previous megatrials in patients with heart failure have demonstrated that drugs stimulating cardiovascular function aggravate long-term survival, whereas those inhibiting cardiovascular function improve survival. Based on these studies, we hypothesize that stimulating vagal activity using a bionic negative feedback control system decreases mortality.

To examine this hypothesis, we conducted experiments in rats with severe heart failure. Hemodynamics

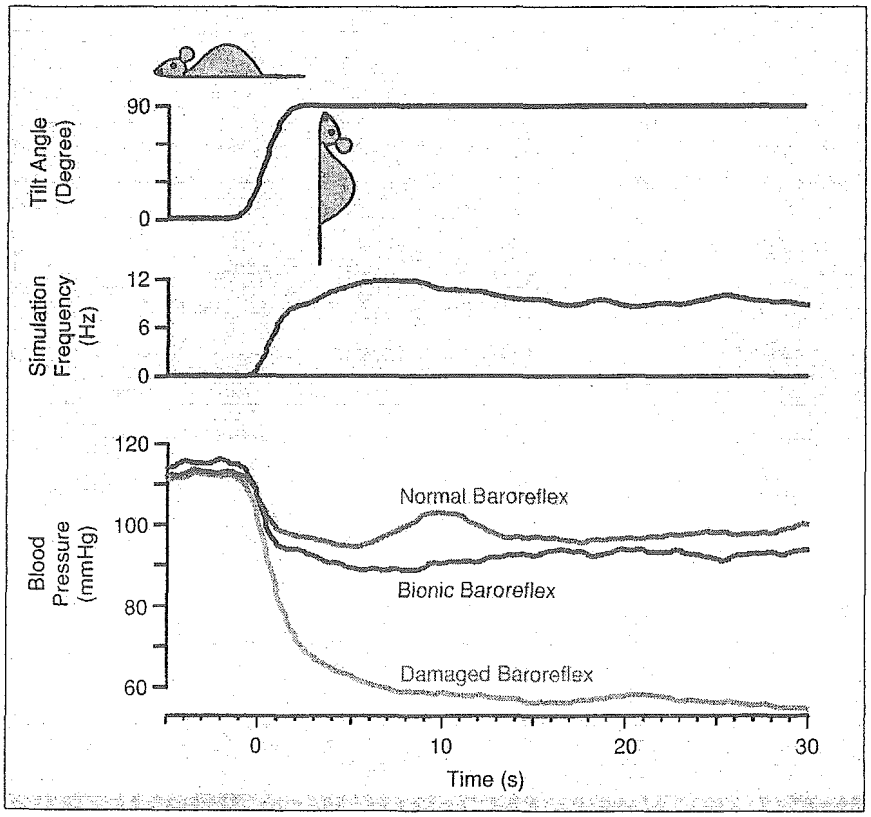

Fig. 8. An example that illustrates how the activation of the bionic brain improves pressure stabilization; it prevents orthostatic hypotension (modified from (3)).

Replacement of lost native function or correction of abnormal native function requires comprehensive identification of the normal cardiovascular regulatory system.

and remodeling were examined in 26 rats, while survival was examined in 52 rats.

In eight-week-old male Sprague-Dawley (SD) rats anesthetized with 1% halothane, the chest was opened and the left coronary artery was ligated at 2–3 mm from its origin. The coronary ligation procedure produced a large myocardial infarct (40–50%), followed by remodeling of the heart and eventually severe heart failure. Since these rats were highly susceptible to ventricular fibrillation, we used mechanical defibrillation by cardiac massage if necessary. If the animal survived the acute period, the chest was closed and the animal was allowed to recover.

After one week, surviving rats were randomized to two groups: a bionic treatment group with vagal stimulation and a control group. These animals underwent another surgery under halothane anesthesia. In the bionic treatment group, we isolated the right cervical vagus nerve and attached a bipolar electrode to be used for telestimulation. We also implanted two devices: a miniature radio-controlled electrical stimulator (telestimulation device) and a blood pressure telemetric device for heart rate monitoring. In the control group, we only isolated the right cervical vagus nerve without implanting any device.

One week after the second surgery, the surviving rats in the bionic treatment group received right vagal stimulation to achieve a target reduction in heart rate (Figure 9). Vagal stimulation was continued for six weeks (two to eight weeks after coronary ligation), with the target heart rate set at 10–20% (20–30 beats/min) lower than the control. The stimulation consisted of a current pulse with an amplitude of 0.1–0.13 mA, pulse width of 0.2 ms, and repetition frequency of 20 Hz. Vagal stimulation was delivered intermittently, for 10 s/min.

At six weeks, vagal stimulation was terminated, and hemodynamic and echocardiographic measurements were obtained under halothane anesthesia. Hemodynamics were obtained using a 2-Fr catheter tipped micromanometer inserted via an apical stab wound. The animals were sacrificed, and the heart weights were measured.

To examine survival, the animals were observed for 14 weeks after vagal stimulation was terminated, a total of 20 weeks (140 days) of observation.

Hemodynamics were examined in 12 rats from the bionic treatment group and 14 rats from the control group [Figure 10(a)]. Infarct size was quantified by histological examination of the ratio of the infarct area to the short-axis cross-sectional area of myocardium. No significant difference in infarct size was observed between the two groups (46 ± 9% in the bionic treatment group, 43 ± 10% in the control group). Heart weight (normalized by body weight, *HW/BW*) was significantly lower in the bionic treatment group (2.71 ± 0.24 g/Kg, $p < 0.05$) than in the control group (3.01 ± 0.31 g/Kg), indicating that cardiac remodeling was inhibited by the bionic treatment with vagal stimulation. The ratio of inhibition in heart weight increase was equivalent to the amount observed in rats receiving angiotensin-converting enzyme inhibitors. Left ventricular contractility was evaluated by the maximal first derivative of left ventricular pressure ($LV + dP/dt$ max). This index was significantly larger (4,206 ± 244 mmHg/s, $p < 0.001$) in the bionic treatment group than in the control group (2,999 ± 173 mmHg/s), indicating preserved function of the noninfarct myocardium. Left ventricular filling pressure (left ventricular end-diastolic pressure, LVEDP) tended to be lower (17 ± 6 mmHg versus 23 ± 5 mmHg) and echocardiographically determined fractional shortening of the left ventricle tended to be larger (15 ± 4%

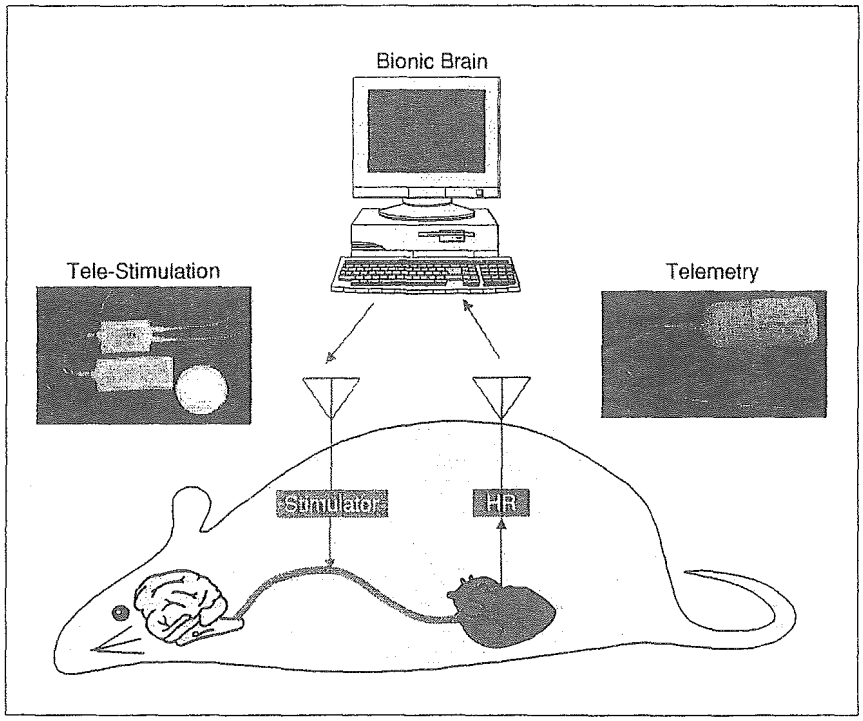

Fig. 9. Animal preparation to depict the bionic treatment of heart failure with vagal stimulation. Heart rate (HR) was continuously monitored by the pressure telemetry while vagal stimulation was delivered by the telestimulation.

One of the methods to achieve appropriate stimulation is to mimic the function of the native vasomotor center.

versus 11 ± 3%) in the bionic treatment group.

Survival was examined in 22 rats in the bionic treatment group and 30 rats in the control group [Figure 10(b)] [4]. While the 20-week survival of the untreated group was only 50%, a markedly improved survival rate (86%, $p = 0.008$) was observed in the bionic treatment group with vagal stimulation. The bionic treatment achieved a 73% reduction in a relative risk of death. The degree of reduction in the relative risk by the bionic treatment far exceeded those by the conventional therapy with drugs such as angiotensin-converting enzyme inhibitors, beta-adrenergic blockers, and spironolactones. The improved survival persisted for 20 weeks, even though the bionic treatment was stopped at six weeks.

These data indicate that the bionic treatment with vagal nerve stimulation markedly improves the long-term survival of rats with heart failure through preventing pumping failure and cardiac remodeling.

The Potential and the Future of Bionic Medicine

We have demonstrated that the bionic cardiovascular medicine permits both the replacement of lost native function and the correction of the abnormal native function. These results demonstrate the efficacy of the new treatment framework, particularly for various incurable diseases.

These results indicate the importance of the regulatory system in the maintenance and progression of various cardiovascular diseases. Furthermore, the success of bionic medicine opens up a new treatment strategy that might be called *functional reconstruction*. This is in stark contrast with the conventional treatment strategy, namely, the etiology-oriented treatment. Since efforts to identify the true cause of a disease often fail, and the cause, even if identified, may not be removable, the new treatment strategy of functional reconstruction serves as a useful alternative modality to combat various incurable diseases.

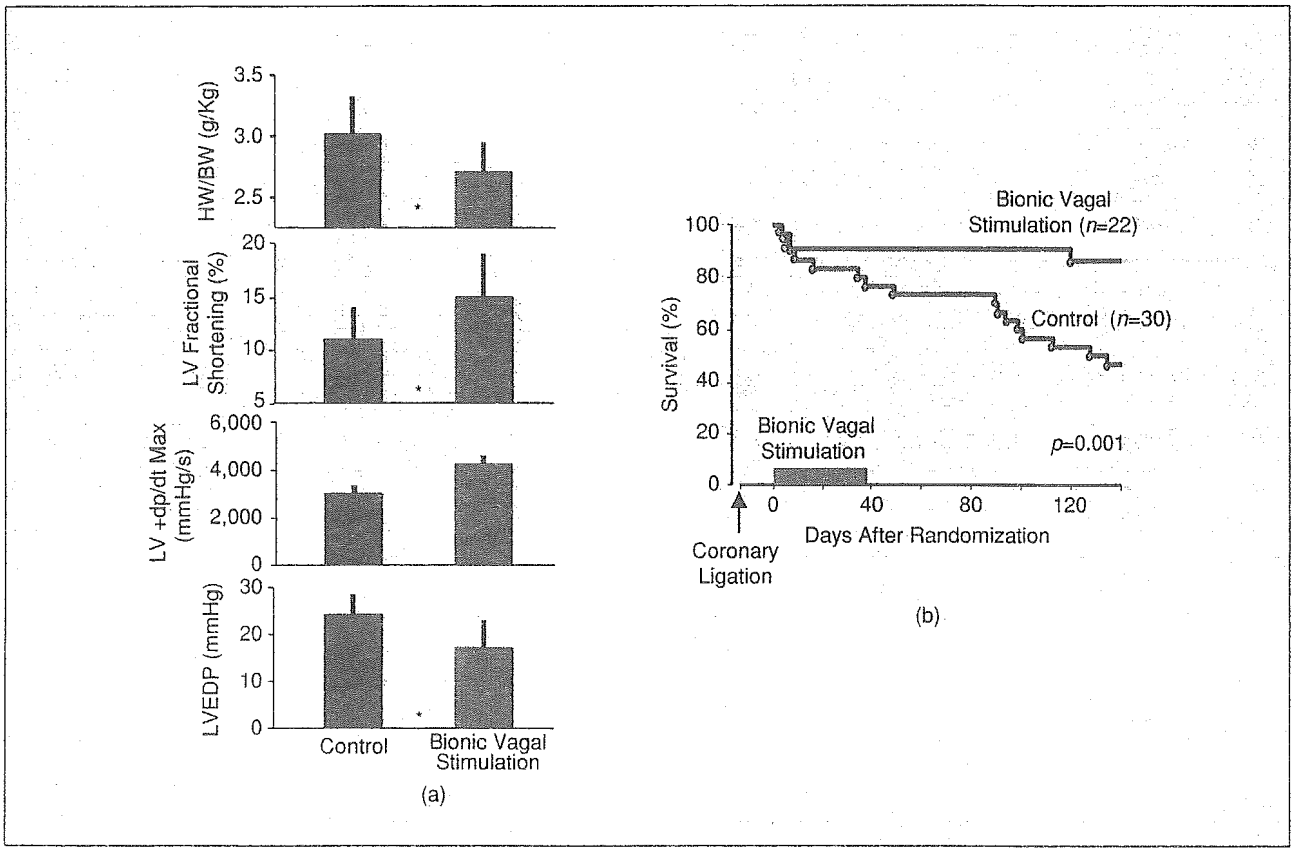

Fig. 10. Long-term bionic treatment of heart failure prevented cardiac remodeling and pumping failure and improved survival. HW, heart weight; BW, body weight; LV, left ventricular; +dP/dt max, maximal first derivative of pressure; EDP, end-diastolic pressure (modified from (4)).

Long-term continuous treatment (manipulation or modification of cardiovascular function) by means of implantable electronics is quite feasible. The measurement of biosignals and the electrical stimulation of biological tissue can be achieved using low-power electronic circuits. Implantation of devices with appropriate treatment logic and close patient monitoring with wireless telecommunication would greatly enhance the therapeutic effects during daily life outside the hospital. At the same time, continuous treatment would reduce the rate of hospital visits and save resources for the medical service.

Finally, the bionic treatment reduces the mortality of rats with heart failure to an extent not achieved by popular cardiovascular drugs. It also appears to be useful in inhibiting fatal cardiac arrhythmias. Based on these findings, the bionic treatment is a most promising approach in improving survival as well as the quality of life of patients with life-threatening cardiovascular diseases.

Acknowledgments

This study was supported by the Health and Labour Sciences Research Grant for Research on Advanced Medical Technology (H14-nano-002) and for Analyzing, Supporting, and Substituting the Function of Human Body (H15-physi-001) from the Ministry of Health Labour and Welfare of Japan and the Program for Promotion of Fundamental Studies in Health Science of the Organization for Pharmaceutical Safety and Research of Japan.

Masaru Sugimachi is the director of the Department of Cardiovascular Dynamics, National Cardiovascular Center Research Institute, Osaka, Japan. He received his M.D. in 1984 from Kyushu University, Japan, and his Ph.D. in biomedical engineering from Kyushu University in 1992. From 1992–2004, he was at the Department of Cardiovascular Dynamics, the National Cardiovascular Center, Osaka, where he integrated the research team for the clinical application of bionic cardiology. He has published more than 100 original papers in cardiac mechanics, cardiovascular regulation, modeling of biological systems, and bionic medicine. He is currently the principal investigator of four major national research projects where he has been developing intelligent implantable cardiac autonomic neuroregulators to treat heart failure, distributed micropacemakers, a next generation implantable cardioverter defribrillator (ICD), and an intensive cardiac care autopilot system.

Kenji Sunagawa is the chair and professor of the Department of Cardiovascular Medicine, Graduate School of Medical Sciences, Kyushu University, Fukuoka, Japan. He has been a member of the administrative committee of the Japanese Society of Medical Electronics and Biological Engineering. He received his M.D. in 1974 from Kyushu University and his Ph.D. in biomedical engineering from Kyushu University in 1985. In 1978, he joined the Department of Biomedical Engineering at Johns Hopkins Medical School where he established the concept of ventricular-arterial coupling. The coupling concept has been adopted for many textbooks of cardiology and cardiac physiology worldwide. From 1992–2004, he chaired the Department of Cardiovascular Dynamics at the National Cardiovascular Center, Osaka, Japan, and developed the basis of bionic cardiology.

Address for Correspondence: Masaru Sugimachi M.D., Ph.D., Department of Cardiovascular Dynamics, National Cardiovascular Center Research Institute 5-7-1 Fujishirodai, Suita, Osaka 565-8565 Japan. Phone: +81 6 6833 5012. Fax: +81 6 6835 5403. E-mail: sugimach@ri.ncvc.go.jp.

References

[1] Y. Ikeda, M. Sugimachi, T. Yamasaki, O. Kawaguchi, T. Shishido, T. Kawada, J. Alexander, Jr., and K. Sunagawa, "Explorations into development of a neurally regulated cardiac pacemaker," *Amer. J. Physiol.*, vol. 269, no. 6, pp. H2141–H2146, Dec. 1995.

[2] T. Sato, T. Kawada, T. Shishido, M. Sugimachi, J. Alexander, Jr., and K. Sunagawa, "Novel therapeutic strategy against central baroreflex failure: A bionic baroreflex system," *Circulation*, vol. 100, no. 3, pp. 299–304, Jul. 1999.

[3] T. Sato, T. Kawada, M. Sugimachi, and K. Sunagawa, "Bionic technology revitalizes native baroreflex function in rats with baroreflex failure," *Circulation*, vol. 106, no. 6, pp. 730–734, Aug. 2002.

[4] M. Li, C. Zheng, T. Sato, T. Kawada, M. Sugimachi, and K. Sunagawa, "Vagal nerve stimulation markedly improves long-term survival after chronic heart failure in rats," *Circulation*, vol. 109, no. 1, pp. 120–124, Jan. 2004.

[5] P.Z. Marmarelis and V.Z. Marmarelis, *Analysis of Physiological Systems: The White-Noise Approach*. New York: Plenum, 1978.

[6] J.S. Bendat and A.G. Piersol, *Random Data: Analysis and Measurement Procedures*, 3rd ed. New York: Wiley-Interscience, 2000.

[7] M. Sugimachi, T. Imaizumi, K. Sunagawa, Y. Hirooka, K. Todaka, A. Takeshita, and M. Nakamura, "A new method to identify dynamic transduction properties of aortic baroreceptors," *Amer. J. Physiol.*, vol. 258, no. 3, pp. H887–H895, Mar. 1990.

[8] K. Jeffrey, "The next step in cardiac pacing: the view from 1958," *Pacing Clin. Electrophysiol.*, vol. 15, no. 6, pp. 961–967, June 1992.

[9] T. Kawada, Y. Ikeda, M. Sugimachi, T. Shishido, O. Kawaguchi, T. Yamazaki, J. Alexander, Jr., and K. Sunagawa, "Bidirectional augmentation of heart rate regulation by autonomic nervous system in rabbits," *Amer. J. Physiol.*, vol. 271, no. 1, pp. H288–H295, Jul. 1996.

[10] T. Kawada, M. Sugimachi, T. Shishido, H. Miyano, Y. Ikeda, R. Yoshimura, T. Sato, H. Takaki, J. Alexander, Jr., and K. Sunagawa, "Dynamic vagosympathetic interaction augments heart rate response irrespective of stimulation patterns," *Amer. J. Physiol.*, vol. 272, no. 5, pp. H2180–H2187, May 1997.

[11] T. Kawada, M. Sugimachi, T. Shishido, H. Miyano, T. Sato, R. Yoshimura, H. Miyashita, T. Nakahara, J. Alexander, Jr., and K. Sunagawa, "Simultaneous identification of static and dynamic vagosympathetic interactions in regulating heart rate," *Amer. J. Physiol.*, vol. 276, no. 3, pp. R782–R789, Mar. 1999.

[12] A.C. Guyton, T.G. Coleman, and H.J. Granger, "Circulation: Overall regulation," *Annu. Rev. Physiol.*, vol. 34, pp. 13–46, Mar. 1972.

[13] Consensus Committee of the American Autonomic Society and the American Academy of Neurology, "Consensus statement on the definition of orthostatic hypotension, pure autonomic failure, and multiple system atrophy," *Neurology*, vol. 46, no. 5, p. 1470, May 1996.

[14] Y. Ikeda, T. Kawada, M. Sugimachi, O. Kawaguchi, T. Shishido, T. Sato, H. Miyano, W. Matsuura, J. Alexander, Jr., and K. Sunagawa, "Neural arc of baroreflex optimizes dynamic pressure regulation in achieving both stability and quickness," *Amer. J. Physiol.*, vol. 271, pp. H882–H890, Sept. 1996.

[15] K. Sunagawa, Y. Ikeda, T. Kawada, M. Sugimachi, T. Shishido, T. Sato, H. Miyano, W. Matsuura, M. Inagaki, and J. Alexander, Jr., "Dynamic control of arterial blood pressure by the sympathetic baroreflex," *Fundam. Clin. Pharmacol.*, vol. 12, suppl. 1, pp. 23s–28s, June 1998.

[16] T. Sato, T. Kawada, M. Inagaki, T. Shishido, M. Sugimachi, and K. Sunagawa, "Dynamics of sympathetic baroreflex control of arterial pressure in rats," *Amer. J. Physiol. Regul. Integr. Comp. Physiol.*, vol. 285, no. 1, pp. R262–R270, July 2003.

[17] T. Kawada, K. Uemura, K. Kashihara, A. Kamiya, M. Sugimachi, and K. Sunagawa, "A derivative-sigmoidal model reproduces operating-point dependent baroreflex neural arc transfer characteristics," *Amer. J. Physiol. Heart Circ. Physiol.*, vol. 286, no. 6, pp. H2272–H2279, June 2004.

[18] P. Kezdi and E. Geller, "Baroreceptor control of postganglionic sympathetic nerve discharge," *Amer. J. Physiol.*, vol. 214, no. 3, pp. 427–435, Mar. 1968.

[19] M. Nagatsu, F.G. Spinale, M. Koide, H. Tagawa, G. DeFreitas, G. Cooper 4th, and B.A. Carabello, "Bradycardia and the role of beta-blockade in the amelioration of left ventricular dysfunction," *Circulation*, vol. 101, no. 6, pp. 653–659, Feb. 2000.

[20] M.T. La Rovere, J.T. Bigger, Jr., F.I. Marcus, A. Mortara, and P.J. Schwartz, "Baroreflex sensitivity and heart-rate variability in prediction of total cardiac mortality after myocardial infarction. ATRAMI (autonomic tone and reflexes after myocardial infarction) investigators," *Lancet*, vol. 351, no. 9101, pp. 478–484, Feb. 1998.

Japanese Journal of Physiology, 55, 157–163, 2005

Dynamic Characteristics of Carotid Sinus Pressure-Nerve Activity Transduction in Rabbits

Toru KAWADA, Kenta YAMAMOTO, Atsunori KAMIYA, Hideto ARIUMI, Daisaku MICHIKAMI, Toshiaki SHISHIDO, Kenji SUNAGAWA*, and Masaru SUGIMACHI

Department of Cardiovascular Dynamics, Advanced Medical Engineering Center, National Cardiovascular Center Research Institute, Osaka, 565-8565 Japan; and *Department of Cardiovascular Medicine, Graduate School of Medical Sciences, Kyushu University, Fukuoka, 812-8582 Japan

Abstract: The dynamic characteristics of the baroreflex neural arc from pressure input to efferent sympathetic nerve activity (SNA) reveal derivative characteristics in the frequency range of 0.01 to 0.8 Hz (i.e., the baroreflex gain augments with increasing frequency) and high-cut characteristics in the frequency range above 0.8 Hz (i.e., the baroreflex gain decreases with increasing frequency) in rabbits. The derivative characteristics accelerate the arterial pressure regulation via the baroreflex. The high-cut characteristics preserve the baroreflex gain against pulsatile pressure by attenuating the high-frequency components less necessary for arterial pressure regulation. However, to what extent the carotid sinus baroreceptor transduction from pressure input to afferent baroreceptor nerve activity (BNA) contributes to these characteristics remains unanswered. To test the hypothesis that the carotid sinus pressure-BNA transduction partly explains the derivative characteristics but not the high-cut characteristics, we examined the dynamic BNA response to pressure input in the frequency range from 0.01 to 3 Hz by using a white noise analysis in 7 anesthetized rabbits. The transfer function from pressure input to BNA showed slight derivative characteristics in the frequency range from 0.01 to 0.3 Hz with approximately a 1.7-fold increase in dynamic gain, but it showed no high-cut characteristics. In conclusion, the carotid sinus baroreceptor transduction partly explained the derivative characteristics but not the high-cut characteristics of the baroreflex neural arc. The present results suggest the importance of the central processing from BNA to efferent SNA to account for the overall dynamic characteristics of the baroreflex neural arc. [The Japanese Journal of Physiology 55: 157–163, 2005]

Key words: systems analysis, transfer function, baroreflex neural arc.

The carotid sinus baroreflex is among the most important negative feedback systems that stabilize arterial pressure (AP) during daily activity. A knowledge of the dynamic characteristics of a given system is important for an in-depth understanding of the system behavior. In previous studies [1–4], we applied a white noise analysis to the carotid sinus baroreflex in rabbits and assessed the transfer function of the baroreflex neural arc from pressure input to efferent sympathetic nerve activity (SNA). The neural arc transfer function revealed two distinct features. One relates to the derivative characteristics in which the baroreflex gain augments with increasing frequency from 0.01 to 0.8 Hz. The derivative characteristics accelerate the dynamic AP regulation by the carotid sinus baroreflex [1]. The other feature relates to the high-cut characteristics in which the baroreflex gain decreases with increasing frequency above 0.8 Hz [4]. The high-cut characteristics prevent the high-frequency components from saturating the baroreflex central processing and preserve the baroreflex gain against pulsatile pressure. However, whether the carotid sinus

Received on Jun 30, 2005; accepted on Jul 29, 2005; released online on Aug 5, 2005; DOI: 10.2170/jjphysiol.R2122
Correspondence should be addressed to: Toru Kawada, Department of Cardiovascular Dynamics, Advanced Medical Engineering Center, National Cardiovascular Center Research Institute, 5-7-1 Fujishirodai, Suita, Osaka, 565-8565 Japan. Phone:+81-6-6833-5012 (Ext. 2427), Fax: +81-6-6835-5403, E-mail: torukawa@res.ncvc.go.jp

baroreceptor transduction from the pressure input to afferent baroreceptor nerve activity (BNA) or the central processing from the afferent BNA to efferent SNA played a major role in forming derivative and high-cut characteristics remains unanswered.

The dynamic characteristics of the pressure input-nerve activity transduction have been examined by the use of step and sinusoidal inputs [5–7]. Although these classical inputs and resulting outputs are easy to interpret, they have a critical drawback because only limited aspects of the system characteristics can be identified. In other words, the system response to untested input signals cannot be predicted precisely because the untested input signals may have frequency components that the step or sinusoidal input does not have. A white noise input, which is rich in frequency components, is most appropriate for a thorough examination of a given system [8–10]. We have identified the dynamic characteristics from pressure input to aortic depressor nerve activity in rabbits with the white noise analysis [11]. The results of that study suggest that the derivative characteristics of the baroreflex neural arc may be partly attributable to the pressure input-nerve activity transduction, whereas the high-cut characteristics may be primarily attributable to the central processing from BNA to efferent SNA. However, regional differences of the transduction properties have been reported between carotid sinus and aortic baroreceptors [12]. Hence the purpose of the present study was to directly estimate dynamic characteristics of the carotid sinus pressure (CSP)-BNA transduction by using the white noise analysis. The results confirmed the hypothesis that the CSP-BNA transduction partly explained the derivative characteristics, but not the high-cut characteristics.

METHODS

Surgical preparations. The animals were cared for in strict accordance with the Guiding Principles for the Care and Use of Animals in the Field of Physiological Sciences approved by the Physiological Society of Japan. Seven Japanese white rabbits weighing 2.7 to 3.1 kg were anesthetized by intravenous injection (2 ml/kg) of a mixture of urethane (250 mg/ml) and α-chloralose (40 mg/ml), and mechanically ventilated with oxygen-enriched room air. A supplemental dose of these anesthetics was administered continuously (0.5 $ml \cdot kg^{-1} \cdot h^{-1}$) to maintain an appropriate level of anesthesia. AP was monitored by a high-fidelity pressure transducer (Millar Instruments, Houston, TX) inserted via the right femoral artery. Following a midline cervical incision, the right external carotid artery was exposed, ligated at two positions, and sectioned in between to access the tissue between the external and internal carotid arteries. A carotid sinus nerve was identified by using a pair of platinum electrodes and by confirming AP-synchronous activity on a loudspeaker. The nerve was then freed from the platinum electrodes during the following carotid sinus isolation procedure. The right internal carotid artery and other small branches arising from the carotid sinus area were ligated. A catheter (0.6 mm internal diameter, 15 cm long) was introduced from the right common carotid artery, and the carotid sinus blind sac was filled with warmed physiological saline. CSP was measured at the end of the catheter opposite the carotid sinus and was controlled by a servo-controlled piston pump (model ET-126A, Labworks, Costa Mesa, CA). A small amount of leakage from the isolated carotid sinus, if any remained, was replenished from the pump during the experiment. After completing the carotid sinus isolation procedure, we attached a pair of stainless steel wire electrodes to the previously identified carotid sinus nerve (Bioflex wire AS633, Cooner Wire, CA) for the multifiber recording of BNA. The nerve and electrodes were secured with silicone glue (Kwik-Cast, World Precision Instruments, Inc.) for insulation. The preamplified nerve signal was band-pass filtered at 150–1,000 Hz. It was then full-wave rectified and low-pass filtered at 30 Hz to quantify the nerve activity. The left carotid sinus nerve, bilateral aortic depressor nerves, and bilateral vagal nerves were all sectioned. The body temperature of the experimental animal was maintained at approximately 38°C with a heating pad.

In three of the seven animals, the controlled CSP was compared with the actual pressure imposed on the carotid sinus area after the BNA recording experiment had finished. After carefully removing the electrodes and silicone glue, we loosened a ligature to the external carotid artery. A catheter-tip pressure transducer (Millar Instruments, Houston, TX) was then introduced into the carotid sinus from the external carotid artery. A signal from the transducer served as the actual pressure imposed on the isolated carotid sinus area.

Protocols. Random input protocol: We randomly changed CSP to either 80 or 120 mmHg with a switching interval of 50 ms for 15 min in order to estimate the dynamic characteristics of the CSP-BNA transduction.

Stepwise input protocol: We increased CSP from 20 to 180 mmHg every minute with a step size of 20